Algorithms for Sensorless Manipulation Using a Vibrating Surface[*]

Karl-Friedrich Böhringer[1], Vivek Bhatt[2], Bruce Randall Donald[1,3], Ken Goldberg[4]

[1] Robotics & Vision Lab, Dept. of Computer Science, Cornell University, Ithaca, NY 14853

[2] Sibley School of Mechanical and Aerospace Engineering, Cornell University, Ithaca, NY 14853

[3] Robotics Lab, Dept. of Computer Science, Stanford University, Stanford, CA 94305

[4] Alpha Lab, Dept. of Industrial Eng. and Op. Research, University of California, Berkeley, CA 94720

November 15, 1996

Abstract

Existing industrial parts feeders move parts through a sequence of mechanical filters that reject parts in unwanted orientations. These feeders require the design of specialized devices such as baffles, cutouts, nests, or traps for each part. In this paper we describe a programmable apparatus that uses a vibrating surface for sensorless, non-prehensile manipulation, where parts are systematically positioned and oriented without sensor feedback or force closure. The idea is to generate and change the dynamic modes of a vibrating surface. Depending on the node shapes of the surface, the position and orientation of the parts can be actively controlled. Our research goal is to develop a science base for manipulation using programmable force fields.

The vibrating surface creates a two-dimensional force vector field. By chaining together sequences of vector fields, the equilibrium states of a part in the field can be cascaded to obtain a desired final state. We describe efficient polynomial-time algorithms that generate sequences of vector fields for sensorless positioning and orienting of planar parts, and we show that these strategies are complete. Finally we consider parts feeders that can only implement a finite set of vector fields. We show how to plan and execute strategies for these devices, and discuss the tradeoff between mechanical complexity and planning complexity.

1 Introduction

It is often extremely costly to maintain part order throughout the manufacture cycle. For example, instead of keeping parts in pallets, they are often delivered in bags or boxes, whence they must be picked out and sorted. A parts feeder is a machine that orients such parts before they are fed to an assembly station. Currently, the design of parts feeders is a black art that is responsible for up to 30% of the cost and 50% of workcell failures [32, 9, 21, 41, 42]. *"The real problem is not part transfer but part orientation."*, Frank Riley, Bodine Corporation [39, p.316, his italics]. Thus although part feeding accounts for a large portion of assembly cost, there is not much scientific basis for automating the process.

---

[*] A brief preliminary version of this paper was presented at the International Conference on Robotics and Automation (Nagoya, Japan, April 1995).

The most common type of parts feeder is the *vibratory bowl feeder*, where parts in a bowl are vibrated using a rotary motion, so that they climb a helical track. As they climb, a sequence of baffles and cutouts in the track create a mechanical "filter" that causes parts in all but one orientation to fall back into the bowl for another attempt at running the gauntlet [9, 39, 40]. To improve feed rate, it is sometimes possible to design the track so as to mechanically rotate parts into a desired orientation (this is called *conversion*). Related methods use centrifugal forces [21], reciprocating forks, or belts to move parts through the filter [37].

Sony's APOS parts feeder [26] uses an array of nests (silhouette traps) cut into a vibrating plate. The nests and the vibratory motion are designed so that the part will remain in the nest only in one particular orientation. By tilting the plate and letting parts flow across it, the nests eventually fill up with parts in the desired orientation. Although the vibratory motion is under software control, specialized mechanical nests must be designed for each part [31].

The reason for the success of vibratory bowl feeders and the Sony APOS system is the underlying principle of *sensorless manipulation* [19] that allows parts positioning and orienting without sensor feedback. The theory of sensorless manipulation is the science base for developing and controlling such devices.

Despite their popularity, all vibratory feeders mentioned so far have some disadvantages:

1. Parts may get wedged or entangled in filters.
2. Parts may get damaged when dropping back into the bowl, or worn by repeated rejections.
3. Each filter reduces the feed rate, depending on the ratio between rejected and accepted parts.
4. The filters must be redesigned for each new part geometry, a task that usually requires skilled work by human experts.[1]

In the early 1980's, several researchers used sensors to determine the pose of parts delivered by a vibratory track [37]. Sensors such as tactile probes [23, 48], photocells [24], fiberoptic sensors [33], and machine vision systems [25, 44] were employed. Once part pose was determined, air-jets and trapdoors were used to group parts in similar poses.

Singer and Seering [42] proposed several designs for parts feeders where programmed vibration was used to drive parts into a stable configuration. Their methods can be useful for bringing parts into one of several poses where its center of mass is as low as possible. Swanson, Burridge, and Koditschek [45] and Tran, Chan, and Hayward [47] used vibrating surfaces for parts feeding strategies, and achieved dynamic equilibrium states to pose parts.

In this paper, we explore how controlled vibration can be used for a new setup to systematically feed planar parts (i.e. parts with extruded polygonal shapes and low aspect-ratio). The idea is to generate and change dynamic modes in a plate by varying applied frequencies. Depending on the frequency of vibration and the boundary conditions, nodes of different shapes are formed. If planar parts are put on this vibrating plate, they move to the node, and end up in a stable orientation [5]. We develop an analysis whereby given the shape of the node, and the part geometry, the final orientation can be predicted. For our device, we further propose a "sensorless" strategy for part manipulation [19], building on the theory originally developed for feeding parts using parallel-jaw grippers [22], which was recently extended to arrays of microactuators and programmable force fields [8, 7]. Note that manipulation with force fields is a form of non-prehensile manipulation [16, 49, 20, 18, 13]: parts are manipulated without form or force closure.

---

[1] Caine [11] presented an experimental CAD system that assists the construction of track filters for vibratory bowl feeders.

In robotics, *minimalism* [12, 6] has become increasingly influential. Minimalism begins with the proposition that doing task A without resource B is interesting, because doing so proves that B is somehow inessential to the information structure of the task. Thus, minimalism attempts to reduce the resource signature [6] for a task. Taking the "transitive closure" of this proposition would result in finding the minimal configuration of resources required to solve a task. Marc Raibert [34] showed that running machines could be built without static stability. Erdmann and Mason [19] showed how to do dextrous manipulation without sensing. Tad McGeer [29] built a biped, kneed walker without sensors, computers, or actuators. Rod Brooks [10] has developed online algorithms that rely less extensively on planning and world models. Canny and Goldberg [12] have demonstrated robot systems of minimal complexity. Donald et al. [16, 6] have built distributed teams of mobile robots that cooperate in manipulation without explicit communication. The manipulation algorithms presented in this paper attempt to minimize the sensor input and the required hardware.

Our results on equilibrium analysis, planning and manipulation strategies, and computational complexity devolve to an application of the theory of programmable vector fields developed by Böhringer and Donald [7]. This paper applies their algorithmic framework to a new class of vibratory devices. The main characteristics of our device are:
- simple design, with no mechanical filters (addressing disadvantages $1 - 3$)
- programmability (addressing problem 4).

Section 2 gives an overview on our research agenda, from the basic ideas of sensorless manipulation using programmable vector fields, to the use of discrete force fields. Section 3 describes the design of our devices, and the performed experiments. In Section 4 we first investigate the dynamics of small particles on the plate, to deduce the approximate nature of the effective force field generated by the vibrating plate. Then we discuss the dynamic behavior of planar objects in such a force field. In Section 5, this model is used to predict the stable rest configurations (equilibria) for parts on the vibrating plate, and the predictions are compared with experimental results. Section 6 presents manipulation grammars, and demonstrates how they can be used to program our device for sensorless manipulation tasks. We close by giving an outlook on future work and open problems.

2   Research Agenda: Scientific Issues

In a programmable force vector field, the forces generated at each point of the field can be controlled independently. Programmable force vector fields can be used to control a variety of flexible planar parts feeders. These devices can exploit exotic actuation technologies such as arrayed, microfabricated motion pixels [8, 43] or, in the case of this paper, transversely vibrating plates. These new automation designs promise great flexibility, speed, and dexterity — we believe they may be employed to orient, singulate, sort, feed, and assemble parts (see for example Figures 1 and 8). However, since they have only recently been invented, programming and controlling them for manipulation tasks is challenging. Our research goal is to develop a science base for manipulation using programmable force fields.

Since the eighteenth century scientists have studied vibrating plates, which cause particles on the plate to arrange along vibratory nodes in so-called Chladni[2] figures [14]. These nodes in the

---

[2]After the German physicist Ernst Chladni, 1756–1827, whose objective was a schematic approach to the construction of better musical instruments.
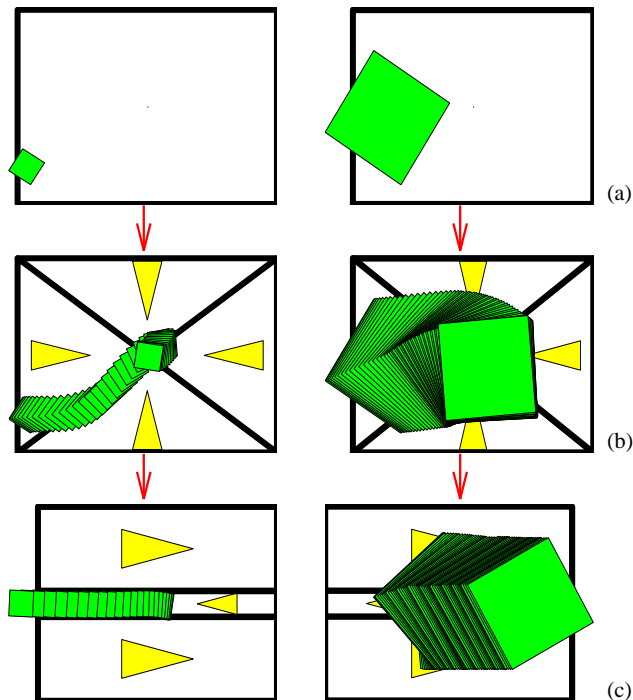
Figure 1: Sensorless sorting using programmable force vector fields: parts of different sizes are first centered and subsequently separated depending on their size.

force fields depend to a large extent on the vibration frequency, and on the location of clamped and free plate edges. Hence by changing the input frequency, or adding software-controlled clamps, specific force fields can be generated.

When a part is placed on our devices, the programmed vector field induces a force and moment upon it. Over time, the part may come to rest in a dynamic equilibrium state. In principle, we have tremendous flexibility in choosing the vector field, since using software-controlled vibratory devices, the force field may be programmed in a fairly fine-grained fashion. Hence, we have a lot of control over the resulting equilibrium states. By chaining together sequences of vector fields, the equilibria may be cascaded to obtain a desired final state — for example, this state may represent a unique orientation or pose of the part. A system with such a behavior exhibits the *feeding property* [2]:

> A system has the *feeding property* over a set of parts $\mathcal{P}$ and a set of initial configurations $\mathcal{I}$ if, given any part $P \in \mathcal{P}$, there is some output configuration $\mathbf{q}$ such that the system can move P to $\mathbf{q}$ from any location in $\mathcal{I}$.

This paper first describes our experimental devices and a technique for analyzing them called *equilibrium analysis*. Then we describe new manipulation algorithms using these tools, and we relax earlier dynamic and mechanical assumptions to obtain more robust and flexible strategies.

2.1 From Continuous Squeeze Fields to Discrete Manipulation Grammars

2.1.1 Sensorless Manipulation Using Continuous Squeeze Fields

We develop our results as follows: In order to discuss planning and control algorithms for the vibrating plate device, first, we make some idealizing assumptions about the kinds of fields it can implement. In particular, we initially assume that it can implement a continuum of "squeeze fields." Next, we further develop a particular simplified dynamic model, called 2PHASE, in which translation and rotation are essentially "decoupled." We then carefully define the computational problem of synthesizing control strategies guaranteed to orient a part from any initial configuration. We find that motion plans with a simple structure suffice.

With current vibratory devices, the rich "vocabulary" required for this idealized model is not attainable. Therefore, we show how our approach generalizes to the practical limitations of our devices, and, in the process, relax our assumptions to include a more realistic dynamic model.

2.1.2 Generalizing to Discrete Manipulation Grammars

We now make the research agenda of Section 2.1.1 precise, and give the reader an overview of our technical results. Previous results on array and force field manipulation strategies may be formalized using *equilibrium analysis.* In [8], Böhringer and Donald proposed a family of control strategies called *squeeze patterns* and a planning algorithm for parts-orientation. This first result proved an $O(n^2)$ upper bound on the number E of orientation equilibria of a non-pathological (see Section 5.1) planar part with n vertices. This yields an $O(E^2) = O(n^4)$ planning algorithm to uniquely orient a part, under certain geometric, dynamic and mechanical assumptions. The strategies employed by these algorithms require significant mechanical and control complexity — even though they require no sensing. The requisite degree of controllability does not exist yet for vibrating plates. For this reason, we introduce and analyze strategies composed of field sequences that we know are implementable using current vibrating plate technology. Each strategy is a sequence of pairs of squeezes satisfying certain "orthogonality" properties. Under these assumptions, we can ensure
  (a) equilibrium stability,
  (b) general first-order dynamics and simple force vector fields, and
  (c) complexity and completeness guarantees.

The framework is quite general, and applies to any set of primitive operations satisfying certain "finite equilibrium" properties — hence it has broad applicability to a wide range of devices. In particular, we view the restricted class of fields as a *vocabulary* and their rules of composition as a *grammar*, resulting in a "language" of manipulation strategies.

Finally, our finite *manipulation grammar* has the following advantage over previous manipulation algorithms for programmable vector fields: previous algorithms such as those described in [8] guarantee to uniquely orient a part, but the translational position of the part is unknown at the strategy's termination. Our new algorithms guarantee to position the part uniquely (up to part symmetry) in translation *as well as* orientation space. Like the algorithms in [8, 7], the new algorithms require no sensing, and work from *any* initial configuration to uniquely pose the part. In particular, the initial configuration is never known to the (sensorless) execution system, which functions open-loop.

The complexity and completeness guarantees we obtain for manipulation grammars are weaker than for the general squeeze field strategies. For squeeze strategies, we apply the algorithmic
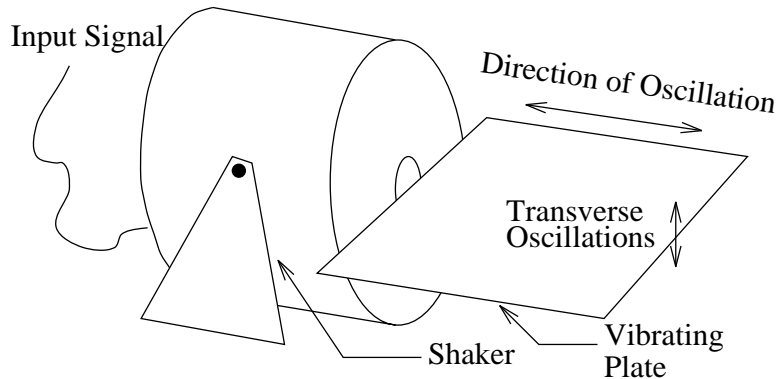
Figure 2: Schematic of experimental setup 1: A 50 $cm \times 40\, cm$ aluminum plate is forced to oscillate horizontally by the shaker armature. The forced oscillation causes a transverse vibration of the plate.

theory of [7] to show that *any* non-pathological planar part with finite area contact can be placed in a unique orientation in $O(E) = O(n^2)$ steps. Under the manipulation grammar, our planner is guaranteed to find a strategy if one exists (if one does not exist, the planner will signal this). However, it is not known whether there exists a strategy for every part. This lack of completeness of manipulation grammar strategies stands in contrast to the *complete* algorithms of [8, 7] for which a *guaranteed* strategy exists for *all* parts. Moreover, the planning algorithm is worst-case exponential instead of merely quadratic in the number of vertices of the part.

3 Experimental Observations

3.1 Setup and Calibration

Figures 2 and 3 are schematics of the experimental setup, which consists of an aluminum plate forced to oscillate in two different configurations. The shaker is a commercially available[3] electrodynamic vibration generator, with a linear travel of $0.02\, m$, and capable of producing a force of up to $500\, N$. The input signal, specifying the waveform corresponding to the desired oscillations, is fed to a single coil armature, which moves in a constant field produced by a ceramic permanent magnet in a center gap configuration.

In the first configuration (Figure 2), the plate is attached to the shaker armature such that it is forced to vibrate in the longitudinal direction (i.e., along the plate axis). For low amplitudes and frequencies, the plate moves with no perceptible transverse vibrations (i.e., vibrations perpendicular to the plate). However, as the frequency of oscillations is increased, transverse vibrations of the plate become more pronounced. The resulting motion is similar to the forced transverse vibration of a rectangular plate, clamped on one edge and free along the other three sides.

The nodes for these transverse oscillations can either be obtained theoretically (Rayleigh [36], Timoshenko [46]), or experimentally using the technique originally pioneered by Chladni [14]. By

---

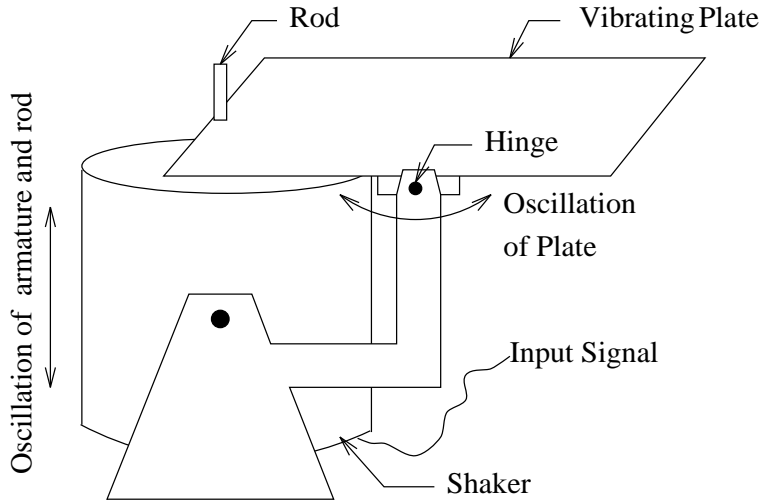[3]Model VT-100G, Vibration Test Systems, Akron, OH, USA.

Figure 3: Schematic of experimental setup 2: The aluminum plate is hinged and can oscillate about an axis in its middle.

sprinkling small sized particles[4] on a vibrating surface, the nodes can be experimentally identified as the regions where the particles tend to collect. The dynamics of "collecting" at the nodes is important in determining the effective force field that leads to the orienting and localization effect of our device, and is discussed in more detail in Section 4.

For the configuration in Figure 2, the location and shape of the node depends on the frequency of vibration. Figure 4 shows experiments to determine the nodes for frequencies of $60\,Hz$ and $100\,Hz$.

The second configuration (Figure 3) forces the plate to undergo transverse vibrations such that the resulting shape of the node, and its location, are independent of the forcing frequency. The plate is hinged about an axis situated midway between, and parallel to, two of its sides. A rod connected to the armature of the shaker forces the plate to an oscillatory motion about the hinged axis. As expected, experimental determination shows that except for a slight distortion due to the effect of clamping at the rod, the node lines up with the hinge axis (Figure 5).

The second setup is run at lower frequencies, to ensure that only the mode where the plate oscillates about the hinge axis is excited. If we increase the operating frequency, modes corresponding to transverse vibration of a plate, clamped at the point of attachment to the rod and the hinged ends, become dominant, and the node shape gets complicated. This effect can be seen at $20\,Hz$ (Figure 5), where the node shows a tendency to get "pulled" towards the point where the plate is clamped to the rod.

3.2   Behavior of Planar Parts

If we put planar parts on the vibrating surface, there is a marked tendency for them to move

---

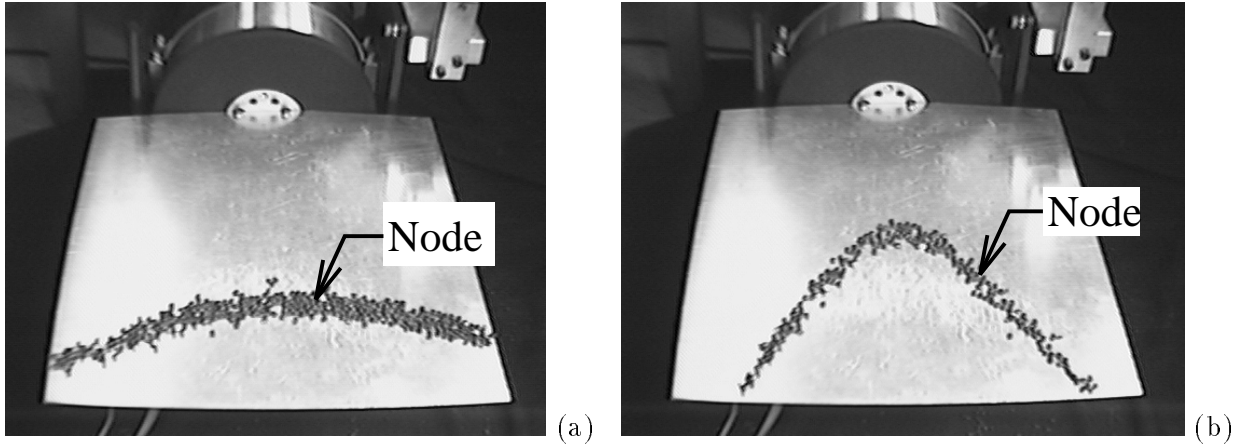[4]Chladni used sand, we use Urad lentils to get a better contrast.

Figure 4: Experimentally determined nodes at (a) 60 Hz and (b) 100 Hz, for experimental setup 1 (see Figure 2). After vibrating the plate for a short time, the particles form Chladni figures, which indicate the location of the vibrational nodes.

towards the node and end up in one of a finite number of stable orientations. We observe the following features over a wide range of frequencies in both the experimental setups:

- From all initial positions on the plate, the objects move towards the node. They end up in a stable position around some point on the node, which depends on the initial position of the object.
- As the object approaches the node (as we show later, after some portion of it crosses the node), there is a tendency for it to rotate until it reaches one of a finite number of stable orientations.

Figure 6 shows two planar shapes, a triangle and a trapezoid, after they have reached their stable position and orientation for the setup in Figure 2. To better illustrate the orienting effect, the curve showing the node has been drawn by hand. Figure 7, similarly shows the stable position of the planar parts for the second setup (Figure 7).

Over the large number of experimental runs performed, there are a couple of qualitative observations describing the ease and speed with which the parts get into a stable configuration:

- At higher frequencies of oscillation, both the velocity of the part towards the node, and the rate of orientation, are relatively faster.
- Objects with a higher degree of rotational asymmetry get into a stable orientation more easily.

Although the location of the node is better identified in the second setup, the lower operating frequencies make the localization of the part at the node, and the corresponding orienting behavior, much slower.

4   Dynamics of Particles and Planar Parts on a Vibrating Plate

The underlying dynamics that causes the objects placed on a vibrating surface to move towards the node give rise to an effective force field. In order to develop a theory for using our device as a
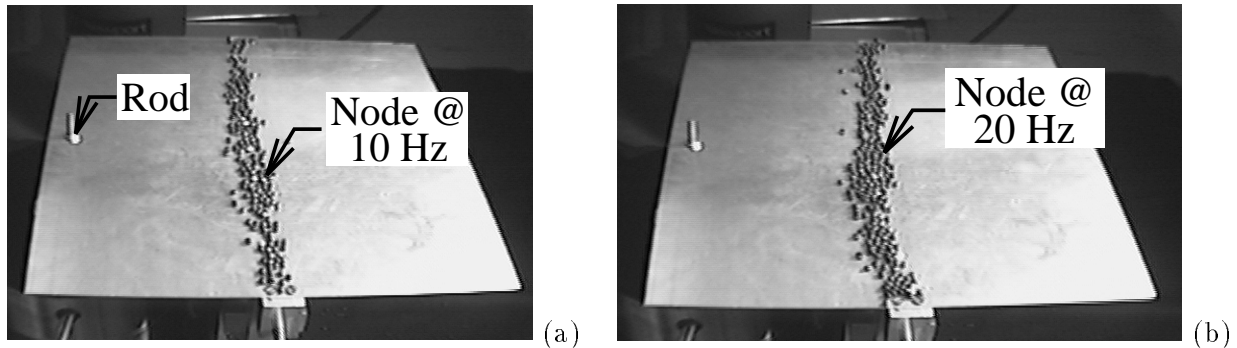
Figure 5: Experimentally determined vibrational nodes at (a) 10 Hz and (b) 20 Hz, for experimental setup 2 (see Figure 3).

viable method for sensorless manipulation, it is important to determine the genesis and variation of this force field over the vibrating plate.

4.1 Chladni Figures

When particles are spread on a vibrating surface, they collect at the nodes, resulting in patterns known as Chladni figures (after Chladni [14], see Figures 4 and 5). Rayleigh [36] describes the motion of the particles towards the nodes in the following words – "*the movement to the nodes is irregular in its character. If a grain be situated elsewhere than at a node, it is made to jump by a sufficiently vigorous transverse vibration. The result may be a movement either towards or from a node; but after a succession of such jumps the grain ultimately finds its way to a node*".

The forces that cause the particles to move to the node act on any object placed on the vibrating surface, generating an effective force field. The underlying dynamics of this phenomenon are very complex. In Appendix A we give an approach towards an analytical model for the more tractable case of the planar motion of a particle bouncing on a string in transverse vibration.

4.2 Motion and Equilibria of Planar Parts

The case of general large objects on the plate is more complicated than individual particles, because the determination of the points on the object that undergo impact, and the resulting impulses, are both difficult problems to solve. For our analysis, we ignore effects such as rolling and tilting of the parts and assume that the contact geometry remains constant over the impacts.

We can consider the planar parts as a rigid arrangement of "particles", each of which interacts with the plate and experiences the effective force field discussed in Section 4.1. The forces have to be summed up over the area of contact, giving a specific force (per unit area), f, that acts at every point of the planar object.

Let P be the planar part in contact with the vibrating plate, and c denote the center of mass of P. The total net force f_P and moment M_P around c can be obtained by integrating the force
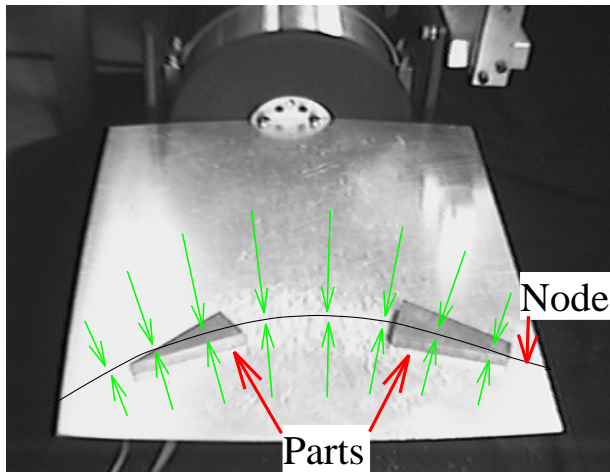
9

Figure 6: Stable position of planar parts in experimental setup 1, at a frequency of $60\,Hz$. The node is marked according to Figure 4.

field f over the contact surface of P:

$$f_P = \int_P f\ dA \tag{1}$$

$$M_P = \int_P (r - c) \times f\ dA \tag{2}$$

Consider a part P on the vibrating plate. We assume that a first-order dynamical system describes the motion of P on the plate. In a first-order system, the velocity of a part is directly proportional to the force acting on it. Hence, an *equilibrium* is a placement of P such that P remains stationary. In an equilibrium, the force and moment acting on P are balanced. This *equilibrium condition* is met when the net force f_P and moment M_P (Equations (1) and (2)) are both zero.

We have made a series of assumptions to suggest that a force field exists for parts on a planar plate. Our experimental results indicate that they are good engineering assumptions when we observe the system over time, due to an averaging effect caused by the vibration of the plate. An "exact" modeling of the impact dynamics between part and plate, even though possible (see e.g. [30, 38]), is not necessary for our purposes.

5   Equilibrium Analysis For Programmable Vector Fields

For the generation of manipulation strategies with programmable vector fields it is essential to be able to predict the motion of a part in the field. Particularly important is determining the stable equilibrium poses a part can reach in which all forces and moments are balanced. This *equilibrium analysis* was introduced in [8], where Böhringer and Donald presented a theory of manipulation for programmable vector fields, and an algorithm that generates manipulation strategies to orient polygonal parts without sensor feedback using a sequence of *squeeze fields*. We now briefly review their algorithm and its complexity bounds.
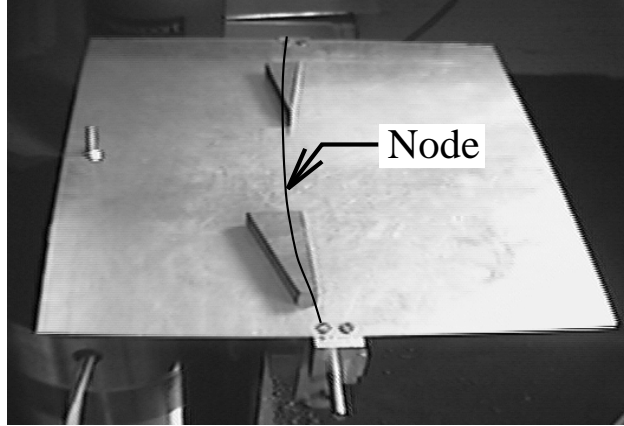
Figure 7: Stable position of planar parts in experimental setup 2, at a frequency of $20\,Hz$. The node is marked according to Figure 5.

5.1 Squeeze Fields and Equilibria

In [8], Böhringer and Donald proposed a family of control strategies called *squeeze fields* and a planning algorithm for parts-orientation.

Definition 1 *Assume l is a straight line through the origin. A* squeeze field f *is a two-dimensional force vector field defined as follows:*
1. *If $z \in \mathbb{R}^2$ lies on l then $f(z) = 0$.*
2. *If z does not lie on l then $f(z)$ is the unit vector normal to l and pointing towards l.*

We refer to the line l as the *squeeze line*, because l lies in the center of the squeeze field.

Assuming quasi-static motion, an object will move perpendicularly towards the line l and come to rest there. We are interested in the motion of an arbitrarily shaped (not necessarily small) part P. Let us call P_1, P_2 the regions of P that lie to the left and to the right of l, respectively, and c_1, c_2 their centers of area. In a rest position both translational and rotational forces must be in equilibrium. We obtain the following two conditions:

I: The areas P_1 and P_2 must be equal.

II: The vector $c_2 - c_1$ must be normal to l.

P has a translational motion component normal to l if **I** does not hold. P has a rotational motion component if **II** does not hold (see Figure 9). This assumes a uniform force distribution over the surface of P, which is a reasonable assumption for planar parts in surface contact.

Definition 2 *A part P is in* translational equilibrium *if the forces acting on P are balanced. P is in* orientational equilibrium *if the moments acting on P are balanced.* Total equilibrium *is simultaneous translational and orientational equilibrium.*

Let (x_0, y_0, θ_0) be an equilibrium pose of P. (x_0, y_0) is the corresponding translation equilibrium, *and θ_0 is the corresponding* orientation equilibrium.
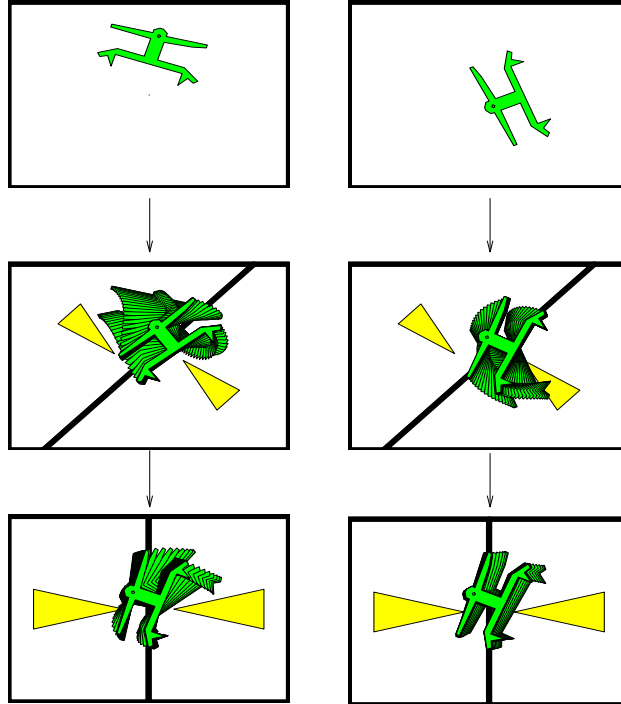
11

Figure 8: Sensorless parts orienting using force vector fields: The part reaches unique orientation after two subsequent squeezes. There exist such orientating strategies for all polygonal parts. See URL `http://www.cs.cornell.edu/home/karl/MicroManipulation` for an animated simulation.

Definition 3 *A* bisector *of a polygon P is a line that cuts P into two regions of equal area.*

Proposition 4 *Let P be a polygon whose interior is connected. There exist $O(k\,n^2)$ bisectors such that P is in equilibrium when placed in a squeeze field such that the bisector coincides with the squeeze linen is the part complexity measured as the number of polygon vertices. k denotes the maximum number of polygon edges that a bisector can cross.*

If P is convex, then the number of bisectors is bounded by $O(n)$.

Proof: Omitted for brevity. For a complete proof see URL `http://www.cs.cornell.edu/home/karl/ProgVecFields`, or [4]. □

For most part geometries, k is a small constant.[5] However in the worst-case, pathological parts can reach $k = O(n)$. A (e.g. rectilinear) spiral-shaped part would be an example for such a pathological case, because every bisector intersects $O(n)$ polygon edges.

5.2 Planning of Manipulation Strategies

In this section we present an algorithm for sensorless parts alignment with squeeze fields [8, 7]. Recall from Section 5.1 that in squeeze fields, the equilibria for connected polygons are discrete

---

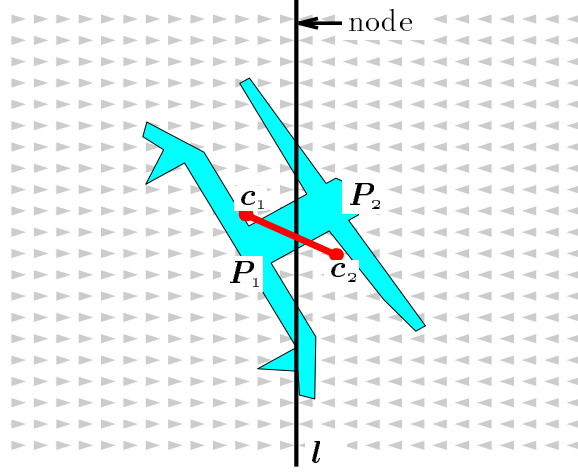[5]In particular, in [8] we assumed that $k = O(1)$.

Figure 9: Equilibrium condition: To balance force and moment acting on P in a unit squeeze field, the two areas P_1 and P_2 must be equal (i.e., l must be a bisector), and the line connecting the centers of area c_1 and c_2 must be perpendicular to the node line.

(modulo a neutrally stable translation parallel to the squeeze line which we will disregard for the remainder of Section 5).

To model their actuator arrays and vibratory devices, the following assumptions are made:

DENSITY: The generated forces can be described by a vector field.

2PHASE: The motion of a part has two phases: (1) Pure translation towards l until the part is in translational equilibrium. (2) Motion in translational equilibrium until orientational equilibrium is reached.

Note that due to the elasticity and oscillation of the actuator surfaces, we can assume continuous area contact, and not just contact in three or a few points. If a part moves while in translational equilibrium, in general the motion is not a pure rotation, but also has a translational component. Therefore, relaxing assumption 2PHASE is one of the key results of this paper.

Definition 5 *Let θ be the orientation of a connected polygon P in a squeeze field, and let us assume that condition $\mathbf{I}$ holds. The* turn function $t : \theta \to \{-1, 0, 1\}$ *describes the instantaneous rotational motion of P:*

$$t(\theta) = \begin{cases} 1 & \text{if } P \text{ will turn counterclockwise} \\ -1 & \text{if } P \text{ will turn clockwise} \\ 0 & \text{if } P \text{ is in total equilibrium (Fig. 10).} \end{cases}$$

See Figure 10 for an illustration. The turn function $t(\theta)$ can be obtained e.g. by taking the sign of the lifted moment $M_P(\mathbf{z})$ for poses $\mathbf{z} = (x, y, \theta)$ in which the lifted force $f_P(\mathbf{z})$ is zero.

Definition 5 immediately implies the following lemma:

Lemma 6 *Let P be a polygon with orientation θ in a squeeze field such that condition $\mathbf{I}$ holds. P is stable if $t(\theta) = 0$, $t(\theta+) \leq 0$, and $t(\theta-) \geq 0$. Otherwise P is unstable.*
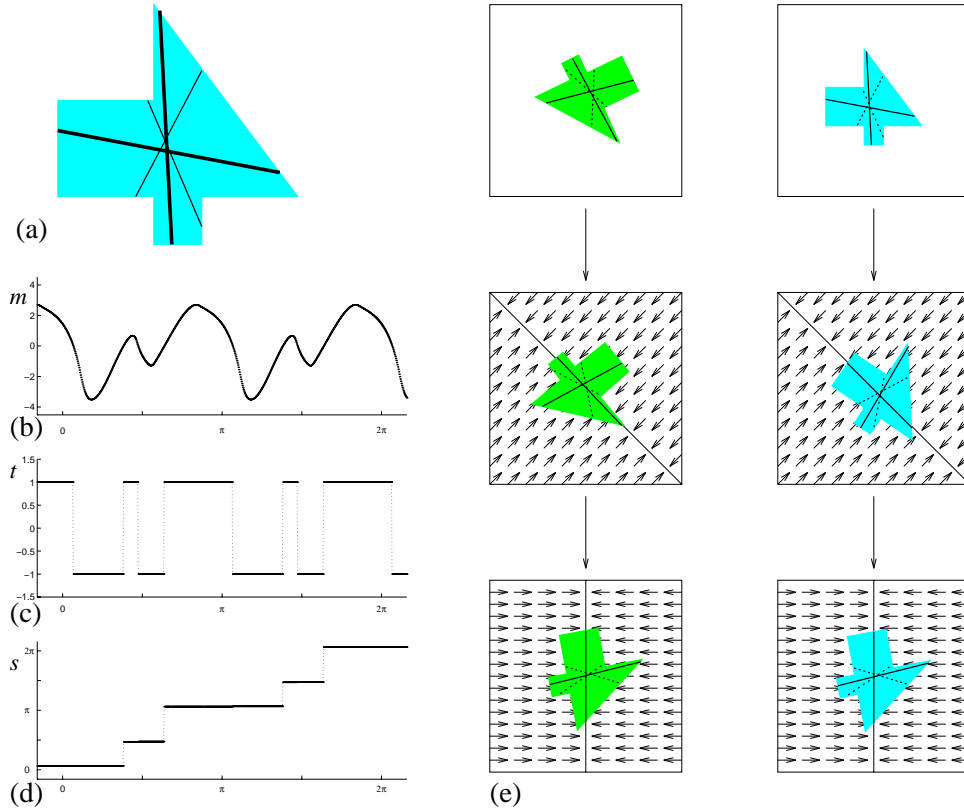
Figure 10: (a) Polygonal part. Stable (thick line) and unstable (thin line) bisectors are also shown. (b) Moment function. (c) Turn function, which predicts the orientations of the stable and unstable bisectors. (d) Squeeze function, constructed from the turn function. (e) Alignment strategy for two arbitrary initial configurations. See URL `http://www.cs.cornell.edu/home/karl/Cinema` for an animated simulation.

Proof: Assume the part P is in a pose (x, y, θ) such that condition **I** is satisfied. This implies that the translational forces acting on P balance out. If in addition $t(\theta) = 0$, then the effective moment is zero, and P is in total equilibrium. Now consider a small perturbation $\delta_\theta > 0$ of the orientation θ of P while condition **I** is still satisfied. For a stable equilibrium, the moment resulting from the perturbation δ_θ must not aggravate but rather counteract the perturbation. This is true if and only if $t(\theta + \delta_\theta) \leq 0$ and $t(\theta - \delta_\theta) \geq 0$. □

Using this lemma we can identify all stable orientations, which allows us to construct the squeeze function [22] of P (see Figure 10d), i.e. the mapping from an initial orientation of P to the stable equilibrium orientation that it will reach in the squeeze field:

Lemma 7 *Let P be a polygonal part on an actuator array $\mathcal{A}$ such that assumptions* DENSITY *and* 2PHASE *hold. Given the turn function t of P, its corresponding squeeze function $s : \mathbb{S}^1 \to \mathbb{S}^1$ is constructed as follows:*

1. All stable equilibrium orientations θ map identically to θ.

14

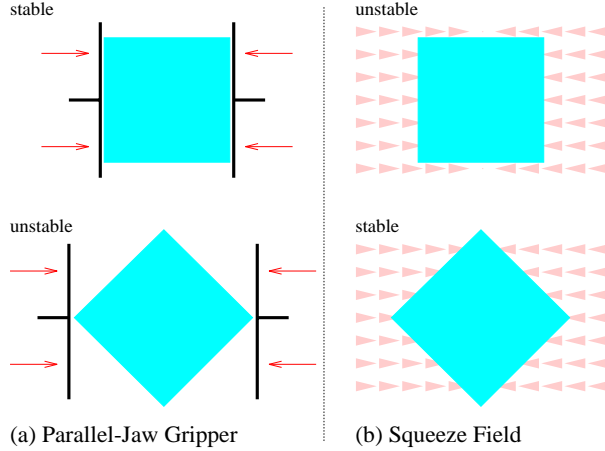(a) Parallel-Jaw Gripper   (b) Squeeze Field

Figure 11: Equilibrium configurations for a square-shaped part using (a) a frictionless parallel-jaw gripper and (b) a MEMS squeeze field. In this example, stable and unstable equilibria are reversed.

> 2. *All unstable equilibrium orientations map (by convention) to the nearest counterclockwise stable orientation.*
>
> 3. *All orientations θ with $t(\theta) = 1$ (-1) map to the nearest counterclockwise (clockwise) stable orientation.*

Then s describes the orientation transition of P induced by A.

Proof: Assume that part P initially is in pose (x, y, θ) in array $\mathcal{A}$. Because of 2PHASE, we can assume that P translates towards the center line l until condition **I** is satisfied without changing its orientation θ. P will change its orientation until the moment is zero, i.e. $t = 0$: A positive moment $(t > 0)$ causes counterclockwise motion, and a negative moment $(t < 0)$ causes clockwise motion until the next root of t is reached.   □

We conclude that any connected polygonal part, when put in a squeeze field, reaches one of a *finite* number of possible orientation equilibria [8, 7]. The motion of the part and, in particular, the mapping between initial orientation and equilibrium orientation is described by the squeeze function, which is derived from the turn function as described in Lemma 7. Note that all squeeze functions derived from turn functions are monotone step-shaped functions.

Goldberg [22] has given an algorithm that automatically synthesizes a manipulation strategy to uniquely orient a part, given its squeeze function. While Goldberg's algorithm was designed for squeezes with a robotic parallel-jaw gripper, in fact, it is more general, and can be used for arbitrary monotone step-shaped squeeze functions. The output of Goldberg's algorithm is a sequence of angles that specify the required directions of the squeezes. Hence these angles specify the direction of the squeeze line in our force vector fields (for example the two-step strategy in Figure 10e).

It is important to note that the equilibria obtained by a force vector field and by a parallel-jaw gripper will typically be different, even when the squeeze directions are identical. For example, consider squeezing a square-shaped part (Figure 11). Stable and unstable equilibria are reversed. This shows that our mechanical analysis of equilibrium is different from that of the parallel-jaw

gripper. Let us summarize these results:

Theorem 8 *Let P be a polygon whose interior is connected. There exists an alignment strategy consisting of a sequence of squeeze fields that uniquely orients P up to symmetries.*

Since the strategies of Theorem 8 consist of fields with squeeze lines at arbitrary angles through the origin, we call them *general $\mathbb{S}^1$ squeeze strategies*, or henceforth *general squeeze strategies*.

Corollary 9 *The alignment strategies of Theorem 8 have $O(k\,n^2)$ steps, and they may be computed in time $O(k^2\,n^4)$, where k is the maximum number of edges that a bisector of P can cross. In the case where P is convex, the alignment strategy has $O(n)$ steps and can be computed in time $O(n^2)$.*

Proof: Proposition 4 states that a polygon with n vertices has $E = O(k\,n^2)$ stable orientation equilibria in a squeeze field ($O(n)$ if P is convex). This means that the image of its corresponding squeeze function is a set of E discrete values. Given such a squeeze function, Goldberg's algorithm constructs alignment strategies with $O(E)$ steps. Planning complexity is $O(E^2)$. □

Goldberg's strategies [22] have the same complexity bounds for convex and non-convex parts, because when using squeeze grasps with a parallel-jaw gripper, only the convex hull of the part need be considered. This is not the case for programmable vector fields, where manipulation strategies for non-convex parts are more expensive. As described in [7], there could exist parts that have $E = \Omega(k\,n^2)$ orientation equilibria in a squeeze field, which would imply alignment strategies of length $\Omega(k\,n^2)$ and planning complexity $\Omega(k^2\,n^4)$.

Note that the turn and squeeze functions have a period of π due to the symmetry of the squeeze field; rotating the field by an angle of π produces an identical vector field. Rotational symmetry in the part also introduces periodicity into these functions. Hence, general squeeze strategies (see Theorem 8) orient a part *up to symmetry*, that is, up to symmetry in the part *and* in the squeeze field. Similarly, the grasp plans based on squeeze functions in [22] can orient a part with a macroscopic gripper only modulo symmetry in the part and in the gripper.[6] Since we reduce to the squeeze function algorithm in [22], it is not surprising that this phenomenon is also manifested for squeeze vector fields as well. For a detailed discussion of parts orientation modulo symmetry see [22].

5.3 Example: Uniquely Orienting Rectangular Parts

To demonstrate the equilibrium analysis from Section 5.1 and the alignment algorithm from Section 5.2, we will generate plans for uniquely orienting several planar polygonal parts (up to part symmetry). In particular, here we will consider the simple case of three rectangles R_{10}, R_{20}, and R_{30}, which have sides a and b such that a is 10, 20, and 30 percent longer than b, respectively (Figure 12).

Our algorithm first determines stable and unstable equilibria of the parts, which correspond to the negative and positive steps in the turn function, respectively (see Lemma 6). The turn function can be obtained as the sign of the moment function, which, for polygonal parts, is a piecewise rational function, and can be derived automatically from the part geometry. For example, consider the rectangle R in Figure 13: A line l through the origin bisects R. If l is placed such that it

---

[6]Parallel-jaw gripper symmetry is also modulo π. Push-squeeze grasps, however, exhibit symmetry modulo 2π.
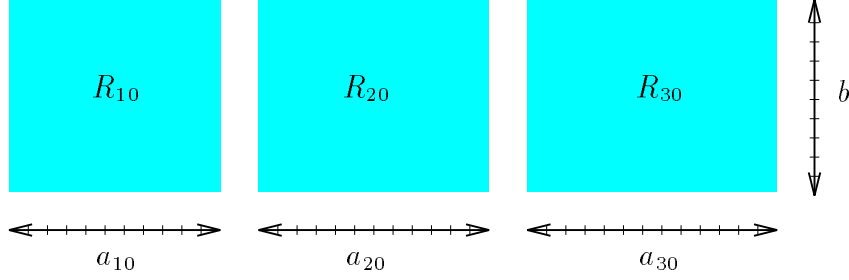
Figure 12: Sample rectangles R_{10}, R_{20}, and R_{30}. Edge a is 10, 20, and 30% longer than edge b, respectively.
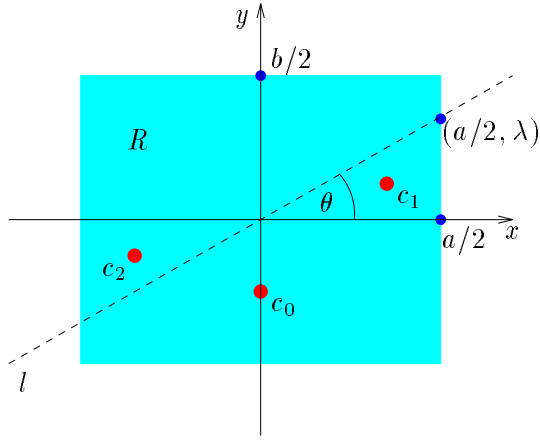

Figure 13: Analytically determining the moment function for a rectangular part R with sides of length a and b. c_0 is the center of mass of the segment below the x-axis. c_1 and c_2 are the centers of the triangular segments between x-axis and line l.

intersects the right edge of R at $(a/2, \lambda)$ with $-b/2 \leq \lambda \leq b/2$, then the COM of the segment below l is

$$
\begin{aligned}
c_\lambda &= \left(\frac{ab}{2} c_0 + \frac{a\lambda}{4}(c_1 - c_2) \right) \frac{2}{ab} \\
&= c_0 + \frac{\lambda}{2b} 2c_1 \\
&= (\frac{a\lambda}{3b}, -\frac{b}{4} + \frac{\lambda^2}{3b})
\end{aligned}
$$

The moment function is the inner product between the vector c_λ, and the direction of the line l. For balanced moment, this product must be zero, which gives us the following condition for equilibrium:

$$
0 = (\frac{a\lambda}{3b}, -\frac{b}{4} + \frac{\lambda^2}{3b}) \cdot (\frac{a}{2}, \lambda)
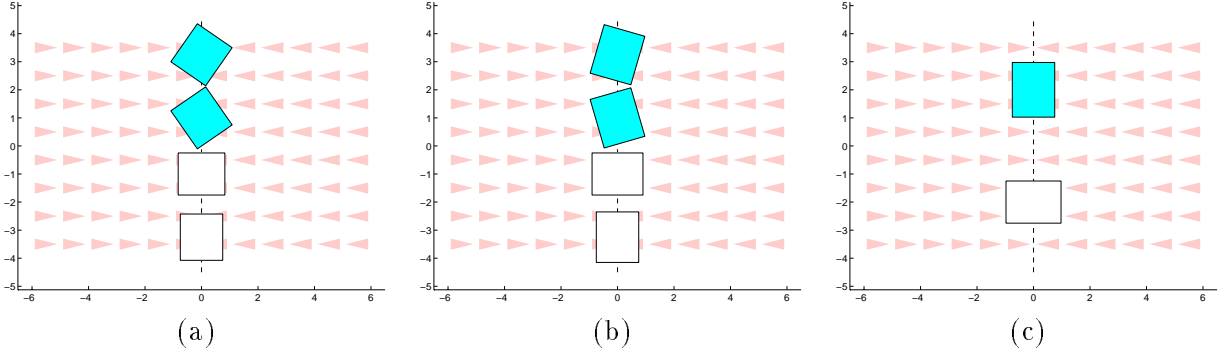$$

Figure 14: Stable (dark) and unstable (white) equilibria of three rectangular parts in a unit squeeze field with vertical squeeze line: (a) R_{10}, edge ratio 1.1; (b) R_{20}, edge ratio 1.2; (c) R_{30}, edge ratio 1.3. R_{10} and R_{20} exhibit two stable equilibria, R_{30} exhibits only one.

Table 1: Equilibria of rectangular parts R_{10}, R_{20}, and R_{30} in a unit squeeze field with vertical squeeze line.

Part	Equilibrium orientations θ	
	stable	unstable
R_{10}	$0.97, 2.18, 4.11, 5.32$	$0, \pi/2, \pi, 3\pi/2$
R_{20}	$1.29, 1.85, 4.43, 4.99$	$0, \pi/2, \pi, 3/pi/2$
R_{30}	$\pi/2, 3\pi/2$	$0, \pi$

$$= \frac{a^2\lambda}{6b} - \frac{b\lambda}{4} + \frac{\lambda^3}{3b}$$

$$= \frac{\lambda}{12b}(2a^2 - 3b^2 + 4\lambda^2)$$

$$\text{So } \lambda = 0$$

$$\text{or } \lambda = \pm\frac{1}{2}\sqrt{3b^2 - 2a^2}$$

$$= \pm\frac{b}{2}\sqrt{3 - 2c^2} \text{ for } a = cb$$

This means that for rectangles with edge ratio $c \leq \sqrt{3/2} \approx 1.22$ (such as R_{10} and R_{20}), there exist equilibrium orientations at angles $\theta = \arctan(\pm\sqrt{3/c^2 - 2})$. For rectangles with larger edge ratio c (such as R_{30}), an equilibrium exists only at $\theta = 0$. A similar analysis can be performed for all other placements of the line l, see [7] for more details. Equilibrium orientations as determined by our planner are shown in Figure 14 and Table 1. Since all of our parts are symmetric with respect to rotation by π, for the remainder of this example we will consider all angles modulo π.

From the equilibrium orientations in Table 1 the algorithm generates the squeeze function, according to Lemma 7. Note that steps in the squeeze function occur at angles corresponding to unstable equilibria, while the image of the squeeze function is the set of all stable equilibrium
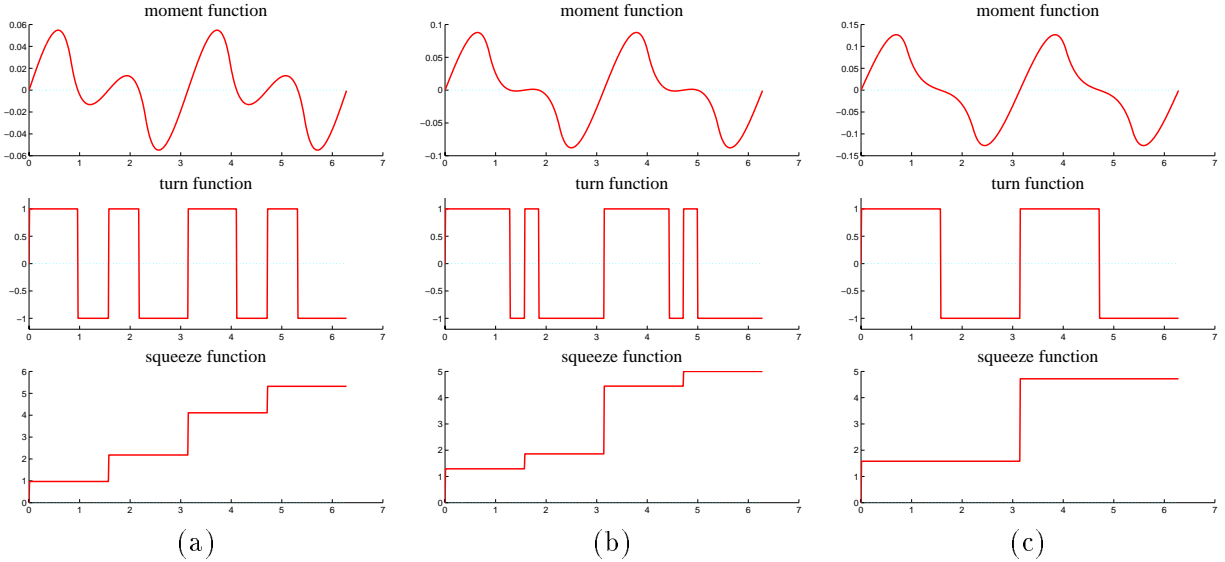
Figure 15: Moment function, turn function, and squeeze function for three rectangular parts: (a) R_{10}, edge ratio 1.1; (b) R_{20}, edge ratio 1.2; (c) R_{30}, edge ratio 1.3. R_{10} and R_{20} exhibit two stable equilibria for θ in the range $[0 \ldots \pi]$, R_{30} exhibits only one.

orientations (see Figure 15).

Finally, the squeeze function is used as input for Goldberg's planning algorithm [22], which returns as output a sequence of squeeze angles. A sequence of two squeeze fields, with a relative angle of $\pi/2$, is sufficient to uniquely orient both R_{10} and R_{20}. See Figure 16 for a sample execution of this plan for two arbitrary initial poses. R_{30} requires only one squeeze field at an arbitrary angle.

It was shown in [7] that this algorithm can uniquely orient arbitrary polygons from any initial configuration (up to part symmetry). However, recall that for this algorithm to work we have made several important assumptions that idealize the practical vibratory feeding devices presented in Section 3.1.

1. 2PHASE assumption, which states that translational and rotational motion of the part is decoupled, implying that the turn function is independent of the initial offset of the part from the squeeze line; see also Section 5.4.

2. Depending on the part shape, the algorithm may generate alignment plans with unit squeeze fields at arbitrary angles. Due to mechanical design limitations, usually not all of these fields will be feasible to implement on most vibratory device setups.

3. The resulting plans uniquely *orient* a part, but the final *translational position* can not be predicted.

In the remainder of this paper, we will investigate new manipulation strategies that address these key issues. In particular, in Section 6 we will develop algorithms for devices with a limited "vocabulary" of available force fields, which will result in a "manipulation grammar" for unique, sensorless posing strategies for arbitrary planar, polygonal parts.
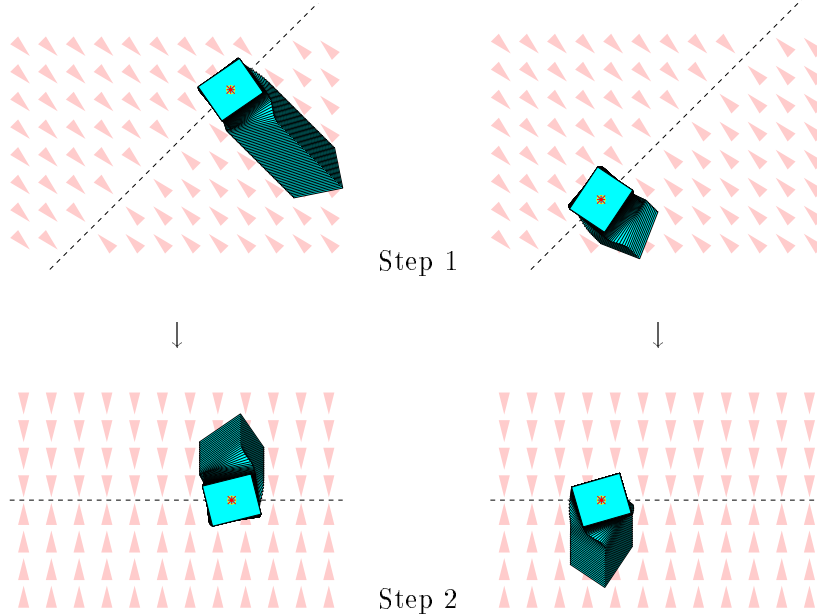
Step 1

↓   ↓

Step 2

Figure 16: Two-step alignment plan for rectangle R_{20}. After two steps, R_{20} reaches a unique *orientation* θ independent of its initial pose. However, the *position* (x, y) is not unique.

5.4 Relaxing the 2Phase Assumption

In Section 5.2, assumption 2Phase allowed us to determine successive equilibrium positions in a sequence of squeezes, by a quasi-static analysis that decouples translational and rotational motion of the moving part. For any part, this obtains a *unique* orientation equilibrium (after several steps). If 2Phase is relaxed, we obtain a dynamic manipulation problem, in which we must determine the equilibria (x, θ) given by the part orientation θ and the offset x of its center of mass from the squeeze line. A stable equilibrium is a (x_i, θ_i) pair in $\mathbb{R} \times \mathbb{S}^1$ that acts as an *attractor* (the x offset in an equilibrium is usually not 0). Again, we can compute these (x_i, θ_i) equilibrium pairs *exactly*, as outlined in Section 5.1.

Considering (x_i, θ_i) equilibrium pairs has another advantage. We can show that, even without 2Phase, after two successive, orthogonal squeezes, the set of stable poses of any part can be reduced from $\mathcal{C} = \mathbb{R}^2 \times \mathbb{S}^1$ to a *finite* subset of $\mathcal{C}$ (the configuration space of part P); see Claim 11 (Section 6.1). Subsequent squeezes will preserve the finiteness of the state space. This will significantly reduce the complexity of a task-level motion planner. Hence if assumption 2Phase is relaxed, this idea still enables us to simplify the general motion planning problem (as formulated e.g. by Lozano-Pérez, Mason, and Taylor in [28]) to that of Erdmann and Mason [19]. Conversely, relaxing assumption 2Phase raises the complexity from the "linear" planning scheme of Goldberg [22] to the forward-chaining searches of Erdmann and Mason [19], or Donald [15].
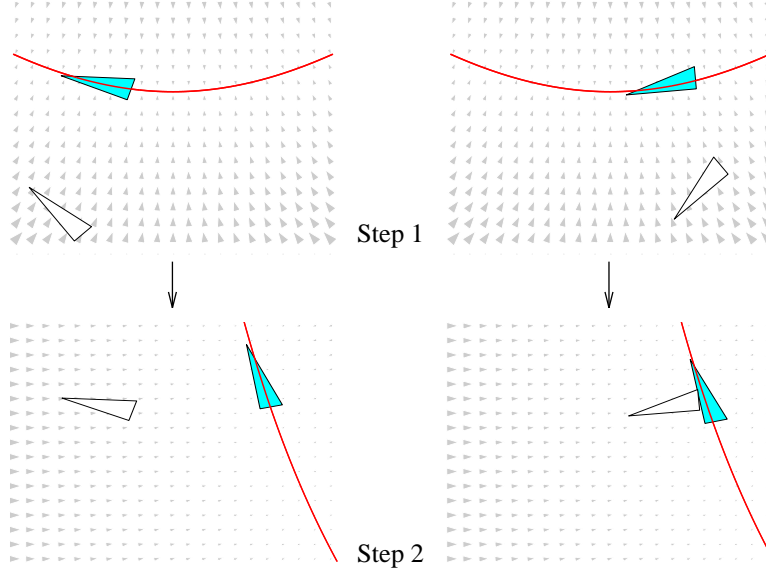
Figure 17: Manipulation vocabulary for a triangular part on a vibrating plate, consisting of two consecutive force fields with slightly curved nodal lines (attractors) which bring the part into (approximately) the same equilibria.

6 Manipulation Grammars

The development of devices that generate programmable vector fields is still in its infancy. For vibrating surfaces the fields are constrained by the vibrational modes of the plate. We are interested in the capabilities of such constrained systems. In this section we give an algorithm that decides whether a part can be uniquely positioned using a given set of vector fields, and it synthesizes an optimal-length strategy if one exists. Furthermore, in Section 6, the vector fields we consider may be arbitrary, and in particular can vary in magnitude (as opposed to unit squeeze fields). If we think of these vector fields as a vocabulary, we obtain a language of manipulation strategies. We are interested in those expressions in the language that correspond to a strategy for uniquely posing the part.

6.1 Finite Field Operators

We define two basic operations on vector fields. Consider two vector fields f and g. $f + g$ denotes point-wise superposition, $f * g$ denotes sequential execution of f, and then g.

Definition 10 *Let P be an arbitrary planar part. A* finite field operator *is a sequence of vector fields that brings P from an arbitrary initial pose into a* finite set *of equilibrium poses.*

A field operator comes with the following guarantee: No matter where in $\mathbb{R}^2 \times \mathbb{S}^1$ the part starts off, it will always come to rest in one of E different total equilibria (Figure 17). That is: for any polygonal part P, either of these field operators is *always* guaranteed to reduce P to a *finite* set of equilibria in its configuration space $\mathcal{C} = \mathbb{R}^2 \times \mathbb{S}^1$.

Claim 11 *Let f and $f_\perp$ be unit squeeze fields such that $f_\perp$ is orthogonal to f. Then the fields $f * f_\perp$ and $f + f_\perp$ induce a finite number of equilibria on every connected polygon P, hence $f * f_\perp$ and $f + f_\perp$ are finite field operators.*

Proof: First consider the field $f * f_\perp$, and w.l.o.g. assume that $f(x, y) = (-\text{sign}(x), 0)$. Also assume that the COM of P is the reference point used to define its configuration space $\mathcal{C} = \mathbb{R}^2 \times \mathbb{S}^1$. As discussed in Sections 5.1 and 5.2, P will reach one of a finite number of orientation equilibria when placed in f or $f_\perp$. More specifically, when P is placed in f, there exists a finite set of equilibria $E_f = \{(x_i, \theta_i)\}$, where x_i is the offset from f's squeeze line, and θ_i is the orientation of P (see Section 5.4). Similarly for $f_\perp(x, y) = (0, -\text{sign}(y))$, there exists a finite set of equilibria $E_{f_\perp} = \{(y_j, \theta_j)\}$. Since the x-component of $f_\perp$ is zero, the x-coordinate of the reference point of P (the COM) remains constant while P is in $f_\perp$. Hence P will finally come to rest in a pose (x_k, y_k, θ_k), where $x_k \in \pi_1(E_f)$, $(y_k, \theta_k) \in E_{f_\perp}$, and π_1 is the canonical projection such that $\pi_1(x, \theta) = x$. Since E_f is finite, so is $\pi_1(E_f)$. $E(f_\perp)$ is also finite, therefore there exists only a finite number of such total equilibrium poses for $f * f_\perp$.

If P is placed into the field $f + f_\perp$, there exists a unique translational equilibrium (x, y) for every given, fixed orientation θ. In each of these translational equilibria, the squeeze lines of f and $f_\perp$ are both bisectors of P. Now consider the moment acting on P when P is in translational equilibrium as a function of θ. Since there are $O(n^2)$ topological placements for a single bisector, therefore there exist also only $O(n^2)$ topological placements for two simultaneous, orthogonal bisectors. In analogy to Proposition 4 in Section 5.1 we can show that for any topological placement of the bisectors, this moment function has at most $O(k)$ roots, where k is the maximum number of edges a bisector of P can cross. This implies that there exist only $O(k\,n^2)$ distinct total equilibria for $f + f_\perp$. □

Corollary 12 *Let f be a finite field operator for a part P, and let g be an arbitrary vector field. Then the sequence $g * f$ is a finite field operator.*

Proof: By definition of a finite field operator, f brings the part P into a finite set of equilibrium poses from arbitrary initial poses, in particular from the poses that are the result of field g. □

Thus by pre-pending an arbitrary sequence of fields to a finite field operator, one can always create a new finite field operator (possibly with a smaller set of discrete equilibria). In the remainder of this section, however, we will only consider finite field operators of minimal length, i.e. field sequences from which no field can be removed without losing the finiteness property (Definition 10).

We have seen in Section 5 that for simple force fields such as e.g. unit squeeze fields, we can predict the motion and the equilibria of a part with exact analytical methods. However, for arbitrary fields such algorithms are not known. Instead we can employ numerical methods to predict the behavior of the part in the force field. These methods are typically numerical computations that involve simulating the part from a specific initial pose, until it reaches equilibrium.[7] We call the cost for such a computation the *simulation complexity* $s(n)$. We write $s(n)$ because the simulation complexity will usually depend on the complexity of the part, i.e., its number of vertices n (for more details also see [17]).

---

[7]See for example URL http://www.cs.cornell.edu/home/karl/Cinema.

Proposition 13 *Consider a polygonal part P, and m finite field operators $\{F_i\}$, $1 \leq i \leq m$, each with at most E distinct equilibria in the configuration space $\mathcal{C}$ for P. There is an algorithm that generates an optimal-length strategy of the form $F_1 * F_2 * \cdots * F_l$ to uniquely pose P up to symmetries, if such a strategy exists. This algorithm runs in $O(m^2 E\ (s(n) + 2^E))$ time, where $s(n)$ is the simulation complexity of P in F_i. If no such strategy exists, the algorithm will signal failure.*

Proof: Construct a transition table T of size $m^2 E$ that describes how the part P moves from an equilibrium of F_i to an equilibrium of F_j. This table can be constructed either by a dynamic analysis similar to Section 5.1, or by dynamic simulation. The time to construct this table is $O(m^2 E\ s(n))$, where $s(n)$ is the simulation complexity, which will typically depend on the complexity of the part.

Using the table T, we can search for a strategy as follows: Define the *state* of the system as the set of possible equilibria a part is in, for a particular finite field operator F_i. There are $O(E)$ equilibria for each finite field operator, hence there are $O(m\, 2^E)$ distinct states. For each state there are m possible successor states as given by table T, and they can each be determined in $O(E)$ operations, which results in a graph with $O(m\, 2^E)$ nodes, $O(m^2 2^E)$ edges, and $O(m^2 E\, 2^E)$ operations for its construction. Finding a strategy, or deciding that it exists, then devolves to finding a path whose goal node is a state with a unique equilibrium. The total running time of this algorithm is $O(m^2 E\ (s(n) + 2^E))$. $\qquad\square$

Hence, as in [19], for any part we can decide whether a part can be uniquely posed using the vocabulary of field operators $\{F_i\}$ but (a) the planning time is worst-case exponential and (b) we do not know how to characterize the class of parts that can be oriented by a specific family of operators $\{F_i\}$. However, the resulting strategies are optimal in length.

This result illustrates a tradeoff between mechanical complexity (the dexterity and controllability of field elements) and planning complexity (the computational difficulty of synthesizing a strategy). If one is willing to build a device capable of general squeeze fields, then one reaps great benefits in planning and execution speed. On the other hand, we can still plan for simpler devices (see Figure 17), but the plan synthesis is more expensive, and we lose some completeness properties.

6.2   Example: Uniquely Posing Planar Parts with Squeeze Fields

In this section we will show how to accomplish tasks with manipulation grammars as developed in Section 6.1. Recall from Section 5.2 that we say a manipulation strategy orients (respectively, poses) a part uniquely if from *any* initial configuration, the part can be brought into a *unique* final orientation (respectively, pose). We will show how the synthesized plans uniquely pose parts from any initial configuration. As an example, suppose our vibratory plate feeder can generate only a very limited vocabulary of four force vector fields, which are also not exactly centered on the plate. For simplicity we assume that the vocabulary consists of unit squeeze fields with squeeze lines at angles of 0, 90, 60 and 150 degrees. We call these fields A, B, C, and D, respectively. The squeeze line of field A is offset by 2 units from the origin, the squeeze line of B is offset by 3 units, and the squeeze lines of C and D intersect at the origin (see Figure 18).

The sequence $A * B$ is a finite field operator, since the squeeze lines of A and B are orthogonal (see Claim 11). In the remainder of this section, we will abbreviate "$A * B$" and simply write "AB". Other finite field operators besides AB are BA, CD, and DC, so that we obtain a vocabulary of $m = 4$ operators.
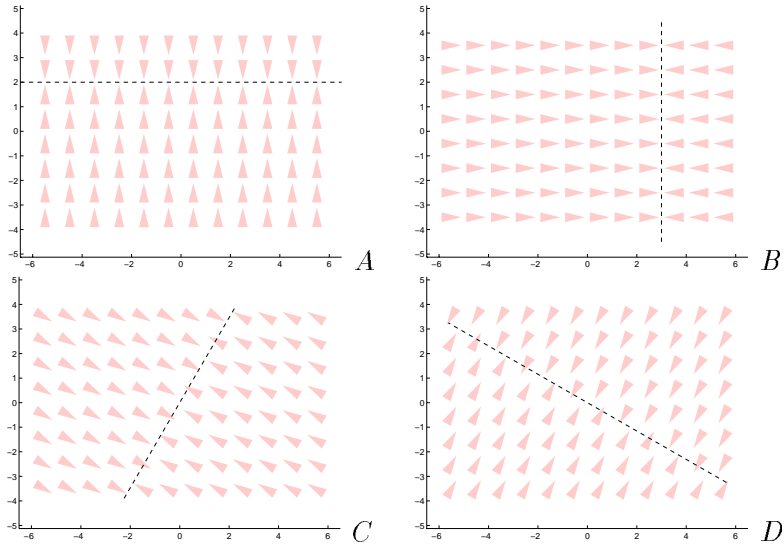
Figure 18: Manipulation vocabulary, consisting of 4 unit squeeze fields.

Note that using unit squeeze fields in this example is not essential; any fields that yield finite sets of equilibria could be used as well. However, for this "didactic" example it is advantageous to use unit squeeze fields because (a) it is easy to determine equilibria for unit squeeze fields, and (b) we can compare the result obtained here with the manipulation plans generated by the planner in Sections 5.2 and 5.3.

6.2.1 Uniquely Posing Rectangles

In this example we will attempt to generate plans for uniquely posing several rectangular parts with the manipulation vocabulary A, B, C, and D (up to part symmetry). As in Section 5.3, we consider three rectangles R_{10}, R_{20}, and R_{30} that have sides a and b such that a is 10, 20, and 30 percent longer than b, respectively (Figure 12). The stable equilibria of R_{10}, R_{20}, and R_{30} in a unit squeeze field were shown in Table 1. Modulo part symmetry, each squeeze field induces only two stable orientation equilibria for R_{10} and R_{20}, and only one stable orientation for R_{30}. Also note that in stable equilibrium, the COM of a rectangle lies on the squeeze line. This gives us a total of $mE = 4 \cdot 2 = 8$ discrete equilibria for R_{10} and R_{20}, when using the finite field operators AB, BA, CD, and DC. All equilibria are shown in Table 2 (compare with Table 1 and Figure 14). Finally, any one of the operators AB, BA, CD, and DC uniquely orients R_{30}, yielding trivial one-step plans to uniquely pose R_{30}. Hence we will omit R_{30} for the remainder of this example.

Given the discrete equilibria, the algorithm based on the constructive proof of Proposition 13 generates a transition table T that describes the mapping between initial equilibrium pose and final equilibrium pose of a part when one finite field operator is applied. This table has mE rows and m columns. Table 3 shows the transitions for parts R_{10} and R_{20}. Each entry in T can be determined either by dynamic analysis, or by simulation. The values in Table 3 were generated by our planner using simulation. Figure 19 shows a trace of such a simulation: The initial pose of part R_{20} is equilibrium $\mathbf{e}_3 = (3, 2, 2.86)$. In field C, R_{20} moves left and up until it reaches an

24

Table 2: Stable equilibria of rectangular parts R_{10} and R_{20} for the manipulation vocabulary AB, BA, CD, and DC.

Operator	Equilibrium	R_{10} (x, y, θ)	R_{20} (x, y, θ)
AB	1	(3,2,0.97)	(3,2,1.29)
	2	(3,2,2.18)	(3,2,1.85)
BA	3	(3,2,2.54)	(3,2,2.86)
	4	(3,2,0.61)	(3,2,0.28)
CD	5	(0,0,2.01)	(0,0,2.34)
	6	(0,0,0.08)	(0,0,2.90)
DC	7	(0,0,0.44)	(0,0,0.77)
	8	(0,0,1.65)	(0,0,1.33)

equilibrium on the squeeze line of C. Subsequently, after field D is applied, R_{20} comes to rest in equilibrium $\mathbf{e}_6 = (0, 0, 2.90)$. In this case, using Claim 11, the equilibria (but not the transitions) can be calculated analytically.

Recall from Section 6.1 that this system has a state space of size $O(m\,2^E)$, because for each of the m finite field operators, there are $O(E)$ discrete equilibria in which the part could be. For example, a state could be "the part is in equilibrium 1, 2, or 4". We can represent such a state as a binary string, "11010000". Hence the transition table T can be used to define a transition graph whose nodes are the $O(m\,2^E)$ states, and whose $O(m^2 E\,2^E)$ edges are derived from the mE transitions in T. A simple breadth-first search of this graph, starting from the state in which all equilibria are possible, will yield optimal-length plans to reach any reachable state.[8] This algorithm will also decide which states are unreachable. Hence it can signal success when the shortest plan to reach a state with a unique equilibrium is found, or signal failure if no such plan exists. Figure 20 shows transition graphs for parts R_{10} and R_{20} with all reachable states, and the shortest paths to reach them from the initial state, in which the part has an arbitrary pose. Notice that there exists a two-step plan for uniquely posing R_{20}, but no such plan exists for R_{10}.

In summary, we observe that with our finite field operators AB, BA, CD, and DC, R_{30} can be uniquely posed in one step, R_{20} requires two steps, while there exists no strategy for R_{10}. Recall that the general squeeze algorithm in Section 5.3 found an alignment strategy for all three rectangles R_{10}, R_{20} as well as R_{30}. However, the algorithm required two squeeze fields at a relative angle of approximately 45°; for R_{10}, it would fail for squeeze lines at a relative angle of 60°. Apparently, parts that are closer to rotational symmetry (i.e., in this case, closer to square-shaped) are more difficult to pose uniquely than more asymmetric (i.e., long rectangular-shaped) parts.

6.2.2   Uniquely Posing and Feeding Arbitrary Parts

In this section we will demonstrate the manipulation grammar algorithm for a more realistic part (see Figure 21a), and for two different manipulation vocabularies. All strategies in this section (and Section 6.2.1) were computed using an automatic planner we implemented, using the techniques

---

[8]We could also imagine using A*-search to improve performance.

Table 3: Transition table for equilibria of the rectangles R_{10} and R_{20}, with finite field operators AB, BA, CD, and DC. For both rectangles, there exist a total of $E = 8$ equilibria, and $m = 4$ finite field operators.

			R_{10}				R_{20}			
			to				to			
			AB	BA	CD	DC	AB	BA	CD	DC
from	AB	1	1	4	6	7	1	4	5	8
		2	2	3	5	8	2	3	5	8
	BA	3	2	3	5	8	2	3	6	7
		4	1	4	6	7	1	4	6	7
	CD	5	2	3	5	8	2	3	5	8
		6	1	4	6	7	2	3	6	7
	DC	7	1	4	6	7	1	4	6	7
		8	2	3	5	8	1	4	5	8

of Section 6.1. We will first extend our manipulation grammar by adding a field F that has a vertical squeeze line at $x = -3$ (Figure 22 left), which yields two new finite field operators, AF and FA. Analysis of the part shows that it has 4 stable orientation equilibria in a unit squeeze field (Figure 21b). It is not difficult to see that, after any two orthogonal squeezes, the part can be in $E = 8$ different poses. We obtain a transition table of size $m^2 E = 228$, which results in a state transition graph with $m\, 2^E = 1536$ nodes (states) and $m^2 2^E = 9216$ edges (transitions). The algorithm finds the following strategy: $CD\ BA\ AF\ FA$, which is equivalent to $CDBAFA$. Two sample executions of this strategy are shown in Figure 23, from different initial poses. A close look at the strategy reveals that operator CD approximately centers the part, such that B can move the part into one of four discrete orientation equilibria below the squeeze line of A. Then A reduces the number of orientation equilibria to two, and F to one (at a unique x-position). Finally, A brings the part into a unique pose: $\mathbf{e}_* \approx (-2.9, 1.9, 3.6)$.

It is important to note the following distinction between the general squeeze strategies for parts orienting of Section 5.2, and the manipulation grammar strategies: As mentioned in Section 5.2, turn and squeeze functions render planning algorithms based upon them susceptible to field symmetries, thereby introducing aliasing in orientation space and admitting completeness and uniqueness proofs of orientation only modulo field symmetry. Since manipulation grammars do not employ turn or squeeze functions, they are immune to this problem, and parts without rotational symmetry can be posed *uniquely*. In essence, turn and squeeze functions assume a global field symmetry. In manipulation grammars, such field symmetries may not exist, e.g. squeeze fields could have arbitrary angles and offsets from the origin. In the first example of this section (Figure 23), the final pose is indeed unique.

As a second example, we add the field G, which has a horizontal squeeze line at $y = -2$ (Figure 22 right), and remove the fields C and D. This results in 8 finite field operators, hence we obtain $m^2 E = 512$ entries in the transition table, $m\, 2^E = 2048$ states and $m^2 2^E = 16384$ transitions. We obtain the strategy $GB\ BA\ AF\ FG$, which is equivalent to $GBAFG$. During
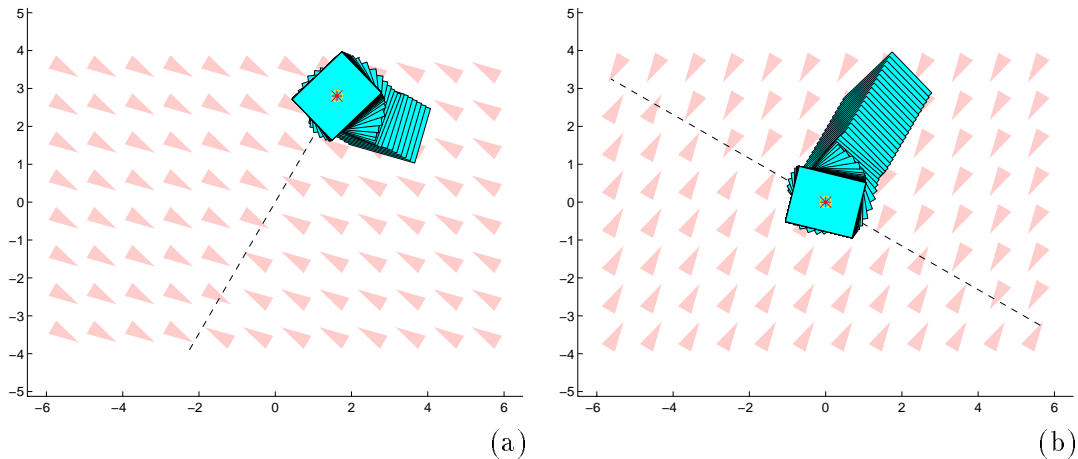
(a) (b)

Figure 19: Simulation of part R_{20} from equilibrium 3 by using finite field operator CD, reaching equilibrium 6: (a) applying field C; (b) applying field D.

execution of this strategy, the COM of the part follows a counterclockwise rectangular path, at each step reducing the number of possible equilibria, until, in the lower left corner, a unique pose is reached (Figure 24). This opens the possibility of *pipelining* the posing process, which could yield more efficient parts feeders: as long as we can ensure that the next part is initially placed sufficiently far to the right so not to interfere with its predecessor, the G field can be used simultaneously for two parts. Hence if the parts feeder periodically cycles through the fields $GBAF$, the next part can be introduced into the device each time *before* G is executed. A part is uniquely posed *after* each execution of G.

6.3 Summary

In this section we have defined manipulation grammars that consist of a vocabulary of planar force vector fields, and we presented an implemented planning algorithm that generates strategies to uniquely position and orient parts. In comparison with the general squeeze strategies of Section 5.2, manipulation grammars allow sets of arbitrary force vector fields, and are not limited to a 1-parameter family of squeeze fields. Consequently, depending on the available manipulation vocabulary, the resulting strategies can be more powerful or more restricted than the orienting strategies generated by the general squeeze algorithm of Section 5.2. In particular, parts can be uniquely posed even when only symmetric force fields are available. As a tradeoff, planning and execution complexity is worst-case exponential instead of merely quadratic in the number of equilibria of the part, and there exist no completeness guarantees that a strategy always exists for a given vocabulary or class of parts. Moreover, numerical simulation was employed to predict the transitions, whereas they may be exactly computed (Section 5.2) for simple squeezes.
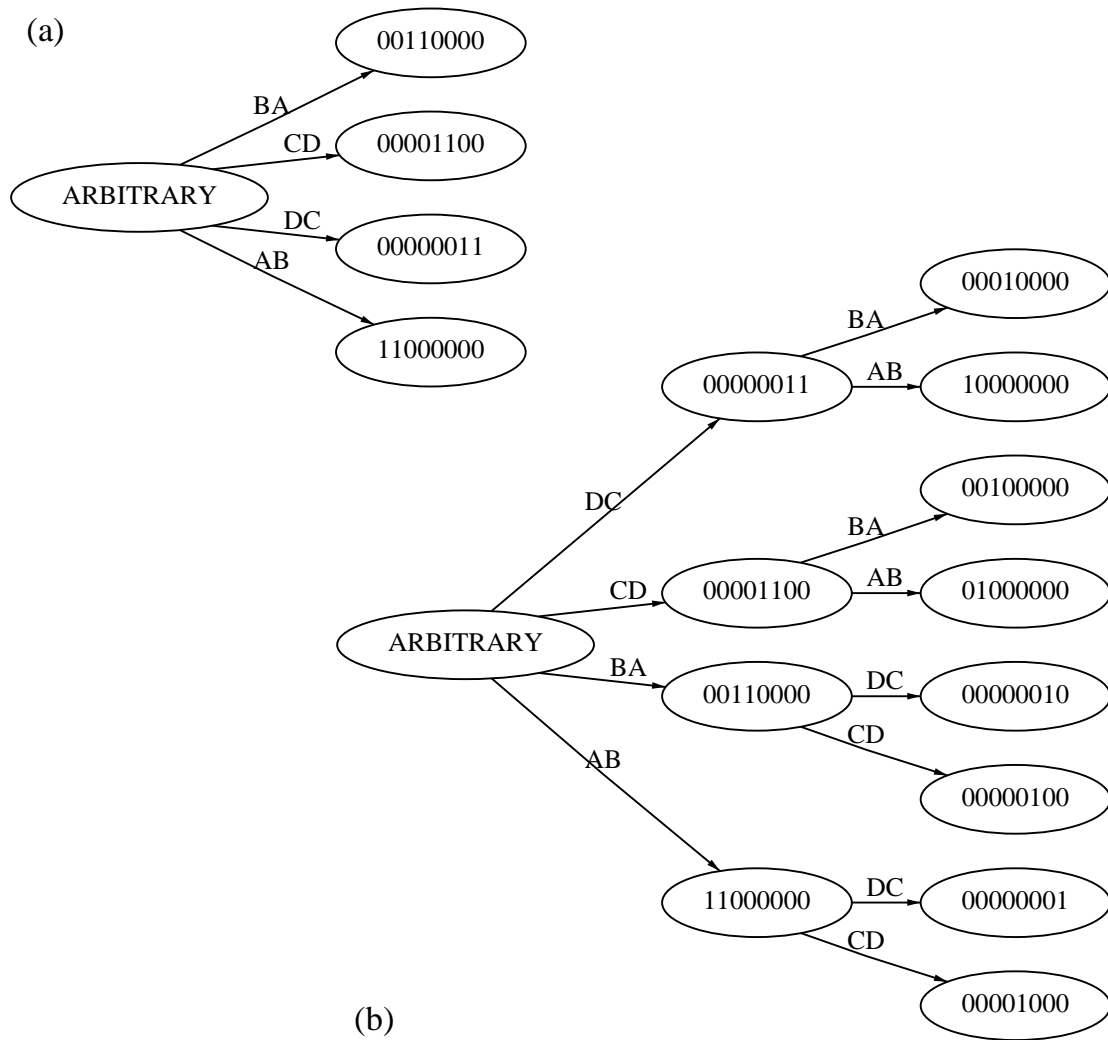
Figure 20: Minimum spanning trees of the state transition graphs for rectangles (a) R_{10}, and (b) R_{20}. All reachable states are shown, as well as the shortest paths to reach each of them. Non-spanning edges (e.g. an edge CD from 11000000 to 00001100) are omitted for simplicity.
(a) No state with unique equilibrium can be reached for R_{10}.
(b) There exist several two-step plans for R_{20} that reach states with unique equilibrium. (Graphs were generated automatically by our planner software.)
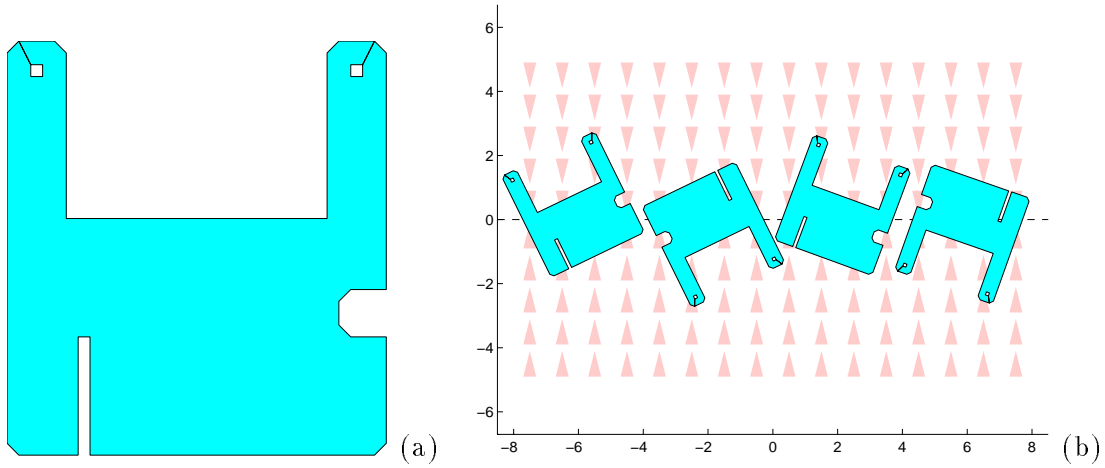
Figure 21: Sample part: (a) nonconvex shape with holes; (b) its four stable equilibria in a unit squeeze field.
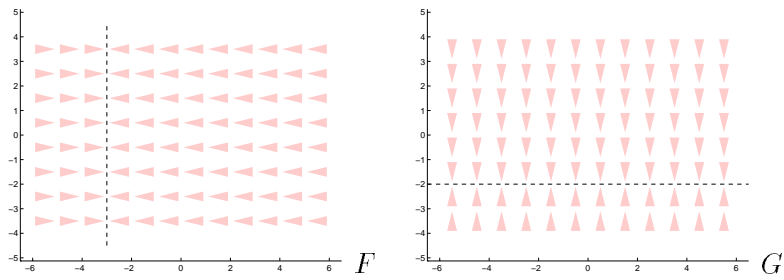
Figure 22: Extensions to the manipulation vocabulary, consisting of 2 unit squeeze fields.
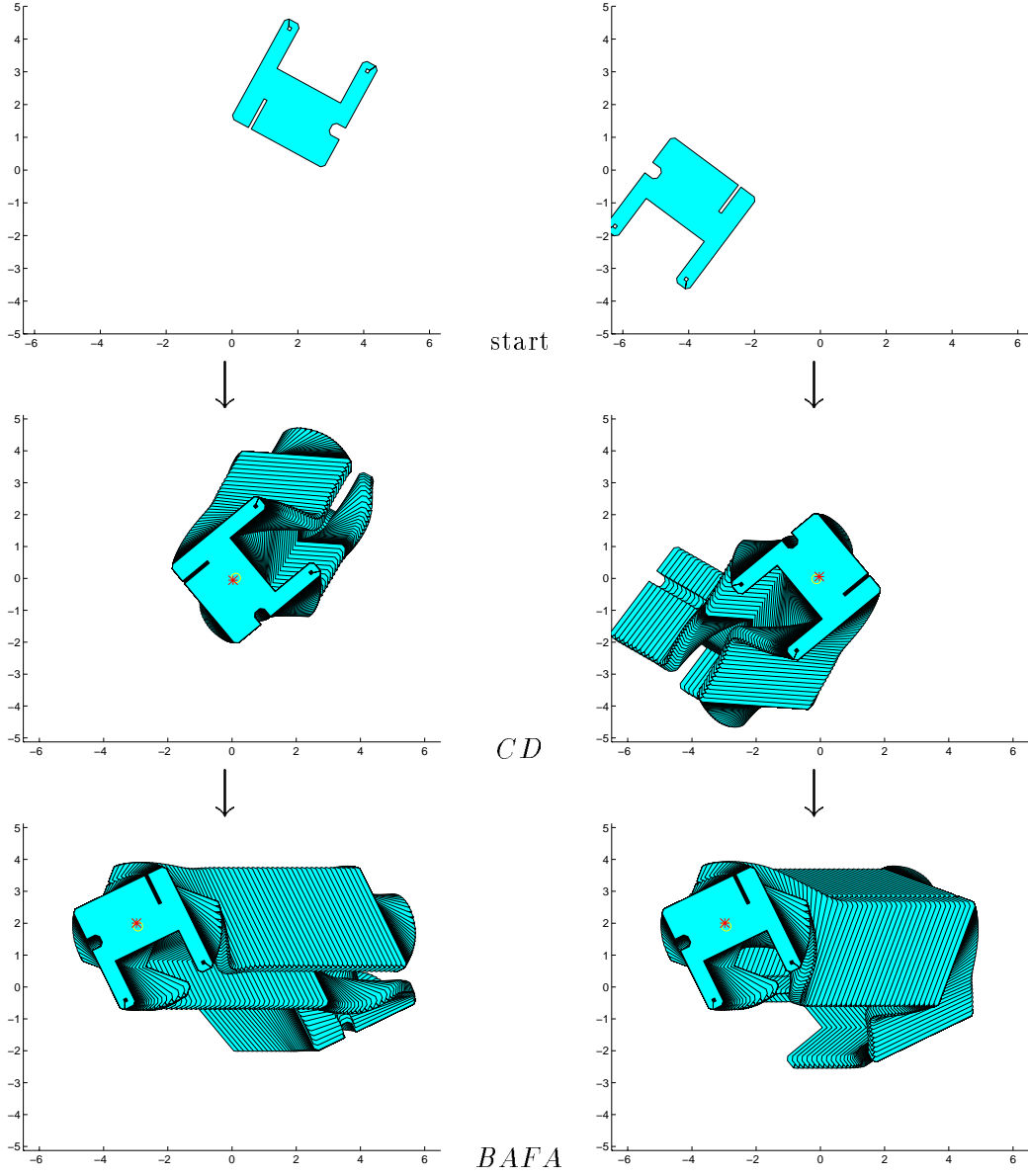
Figure 23: Two sample executions of the manipulation grammar strategy $CD\ BA\ AF\ FA$. For clarity, the simulation trace has been broken up into parts: initial pose (top), motion under CD (middle), and motion under $BA\ AF\ FA$ (bottom). Initial poses: (a) $\mathbf{z}_0 = (2, 2, -0.5)$, (b) $\mathbf{z}_0 = (-4, -1, 2.5)$. Final pose $\mathbf{e}_* \approx (-2.9, 1.9, 3.6)$.
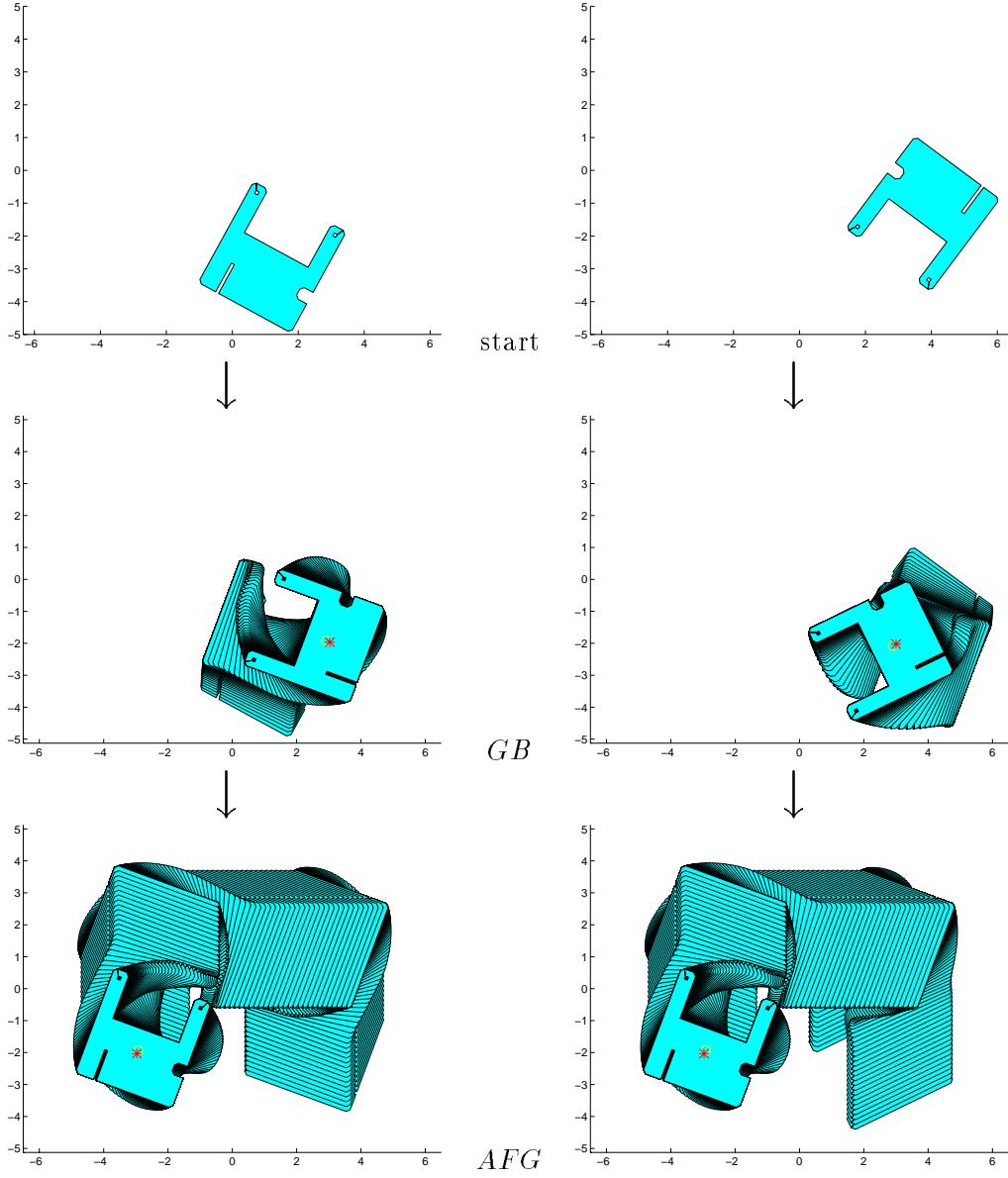
Figure 24: Two sample executions of strategy GB BA AF FG $= GBAFG$. For clarity, the simulation trace has been broken up into parts: initial pose (top), motion under GB (middle), and motion under AFG (bottom). Initial poses: (a) $\mathbf{z}_0 = (1, -3, -0.5)$, (b) $\mathbf{z}_0 = (4, -1, 2.5)$. Final pose $\mathbf{e}_* \approx (-2.9, -1.9, 5.9)$.

31

7　Conclusions and Open Problems

Parts Sorting with Geometric Filters. This paper focuses mainly on sensorless manipulation strategies for *unique positioning* of parts. Another important application of programmable vector fields are *geometric filters* [3, 35], which would be useful for sorting and singulation of parts. Figure 1 shows a simple filter that separates smaller and larger parts. We are interested in the question *Given n parts, does there exist a vector field that will separate them into specific equivalence classes?* For example, does there exist a field that moves small and large rectangles to the left, and triangles to the right? In particular, it would be interesting to know whether for any two different parts there exists a sequence of force fields that will separate them.

Resonance Properties. Preliminary experiments have indicated that by applying frequencies close to the natural frequency of a part, the force field can be tuned very effectively. Is it possible to exploit the dynamic resonance properties of parts to tune the control signal of the surface to perform efficient dynamic manipulation?

Output Sensitivity. We have seen in Sections 5.1 and 6 that the efficiency of planning and executing manipulation strategies critically depends on the number of equilibrium configurations. Expressing the planning and execution complexity as a function of the number of equilibria E, rather than the number of vertices n, is called *output sensitive analysis*. In practice, we have found that there are almost no parts with more than two distinct (orientation) equilibria, even in squeeze fields. This is far less than the $E = O(k\,n^2)$ upper bound derived in Section 5.1. If this observation can be supported by an exact or even statistical analysis of part shapes, it could lead to extremely good expected bounds on plan length and planning time, even for the strategies employing manipulation grammars (note that the complexity of the manipulation grammar algorithm in Proposition 13 is output-sensitive).

Universal Feeder-Orienter (UFO) Devices. It was shown in Proposition 4 that every connected polygonal part P with n vertices has a finite number of stable orientation equilibria when P is placed into a squeeze field S. Based on this property we were able to generate manipulation strategies for unique part alignment. Böhringer and Donald showed in [7] that by using a combined radial and squeeze field $R + \delta S$, the number of equilibria can be reduced to $O(k\,n)$. Using elliptic force fields $f(x, y) = (\alpha x, \beta y)$ such that $\alpha \neq \beta$ and $\alpha, \beta \neq 0$, this bound can be reduced to two [27]. An "inertial" squeeze field $f(x, y) = (-\text{sign}(x)x^2, 0)$ uniquely orients a part modulo field symmetry π. In a stable equilibrium, the part's major principal axis of inertia lines up with the squeeze line to minimize the second moment of inertia.

Does there exist a *universal field* that, for every part P, has only one unique equilibrium (up to part symmetry)? Such a field could be used to build a *universal parts feeder* [1] that uniquely positions a part without the need of a clock, sensors, or programming.

Böhringer and Donald propose in [7] a combined radial and "gravitational" field $R + \delta G$ which might have this property. δ is a small positive constant, and G is defined as $G(x, y) = (0, -1)$. This device design is inspired by the "universal gripper" in [1]. Such a field could be obtained from an array of MEMS (micro electro mechanical system) actuators [7]. Alternatively, a resonating speaker, or a vibrating disk-shaped plate that is fixed at the center, might be used to create a radial force
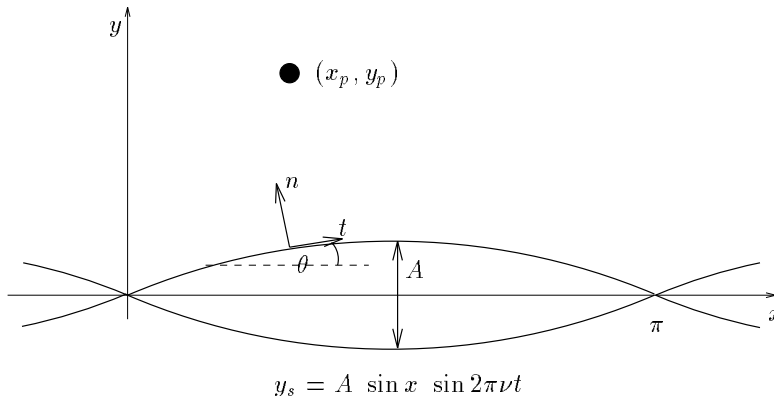
$$y_s = A \ \sin x \ \sin 2\pi\nu t$$

Figure 25: Particle bouncing on a vibrating string.

field. Extensive simulations show that for every part we have tried, one unique total equilibrium is always obtained. We are working toward a rigorous proof of this experimental observation.

APPENDIX

A   Particle Bouncing on a Vibrating String

To understand the effective forces on particles on a vibrating surface, we look at the more tractable case of the planar motion of a particle bouncing on a string in transverse vibrations (Figure 25).

The string vibrates in the first mode, and is not affected by its interaction with the particle. The shape of the string, at time t, for a given x location is:

$$y_s = A \ \sin x \ \sin 2\pi\nu t$$

where ν is the frequency of oscillation. The position of the particle is given by (x_p, y_p).

The interaction between the particle and the string is through a sequence of impacts. We use a model for particle impact with a finite friction coefficient μ, and a coefficient of restitution e. θ is the slope of the string at the point and instant of impact, and is small for small amplitudes of string vibration.

$$\tan\theta = A \ \cos x \ \sin 2\pi\nu t$$

The motion of the particle can be simulated as a series of impacts with the string, with the particle in free flight in-between. The change in the momentum of the particle during impact is calculated using a simple planar impact model. Figure 26 shows the results of a numerical simulation of the model at two different values of e.

For a particle starting at rest, at $t = 0$, we find that $\dot{y}_p \gg \dot{x}_p$. Using the assumption that the amplitude of oscillations is small, $\sin\theta \approx \tan\theta$, $\cos\theta \approx 1$. If $(\dot{x}_p^-, \dot{y}_p^-)$ represent the velocity just
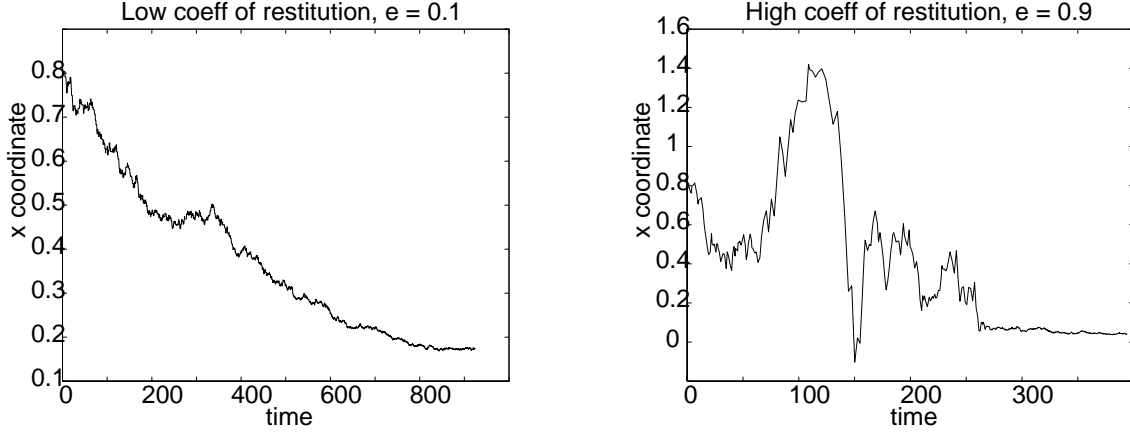
33

Figure 26: Simulation results showing the position of a particle moving on a vibrating string.

before impact, the velocity just after impact $(\dot{x}_p^+, \dot{y}_p^+)$, is:

$$\dot{x}_p^+ \;=\; e\,(\dot{y}_p^- - \dot{y}_s^-)\sin\theta + \alpha\,v_{rel_t}^- \tag{3}$$

$$\dot{y}_p^+ \;=\; \dot{y}_s^-(1+e) - e\,\dot{y}_p^- \tag{4}$$

where $v_{rel_t}^- = (\dot{y}_p^- - \dot{y}_s^-)\sin\theta + \dot{x}_p^-$ is the relative velocity along the tangential direction before impact, and $\alpha \in [0,1]$ is the dissipation factor that depends on μ.

After the impact, $\dot{x}_p^+$ is a sum of the relative tangential velocity before impact, attenuated by friction; and a component from the impulse in the normal direction, which depends on e and the slope of the string at the point of impact. The portion of x impulse added purely due to the effect of the string can be approximated as $-e\,\dot{y}_s\sin\theta$, by setting $\dot{y}_p^- = 0$.

If this component of the impulse were spread uniformly over time, the effective force, F_{eff}, that the particle would experience is:

$$F_{eff} \;\propto\; -\nu e A^2 \sin x \, \cos 2\pi\nu t \, \cos x \, \sin 2\pi\nu t \tag{5}$$

We now use the argument that it is more probable for the particle to impact the string at times when the string is above the mean rest position, to show that over a large number of impacts, the time dependent terms in equation (5) average out to a positive quantity. Therefore, the time averaged effective force, F_{avg}, experienced by the particle is:

$$F_{avg} \;\propto\; -\nu e A^2 \sin 2x$$

This confirms the intuition and the observed behavior that the particle moves faster at higher amplitudes of string oscillation, coefficient of restitution, and oscillation frequency. The sine dependency of the force with x ensures that it points towards the corresponding nodes on either side of the anti-node at $x = \frac{\pi}{2}$.

Further experiments need to be done to study the effect of surface geometry and friction properties on the final part configuration. The analysis can be further developed to determine the nodes

34

and the vibration mode shape for a given plate setup, and the information used in conjunction with the part geometry and surface property to predict the part behavior. We also propose an extension of the experimental setup by adding software-controlled clamps to alter the node shapes in a systematic manner. This will then be combined with automatic calibration of the setup by determining nodes using edge detection, and a planner to automatically generate a plan to get a given part in a desired orientation.

Acknowledgments

References

[1] T. L. Abell and M. Erdmann. A universal parts feeder, 1996. Personal communication / in preparation.

[2] S. Akella, W. H. Huang, K. M. Lynch, and M. T. Mason. Planar manipulation on a conveyor by a one joint robot with and without sensing. In *International Symposium of Robotics Research (ISRR)*, 1995.

[3] E. Arkin, P. Chew, D. Huttenlocher, K. Kedem, and J. Mitchell. An efficiently computable metric for comparing polygonal shapes. *IEEE PAMI*, 1990.

[4] K.-F. Böhringer. *Programmable Force Fields for Distributed Manipulation, and Their Implementation Using Microfabricated Actuator Arrays*. PhD thesis, Cornell University, Department of Computer Science, Ithaca, NY 14853, Jan. 1997. Forthcoming.

[5] K.-F. Böhringer, V. Bhatt, and K. Y. Goldberg. Sensorless manipulation using transverse vibrations of a plate. In *Proc. IEEE Int. Conf. on Robotics and Automation (ICRA)*, pages 1989 − 1996, Nagoya, Japan, May 1995. http://www.cs.cornell.edu/home/karl/VibratoryAlign.

[6] K.-F. Böhringer, R. G. Brown, B. R. Donald, J. S. Jennings, and D. Rus. Distributed robotic manipulation: Experiments in minimalism. In *Fourth International Symposium on Experimental Robotics (ISER)*, Stanford, California, June 1995. http://www.cs.cornell.edu/home/brd.

[7] K.-F. Böhringer, B. R. Donald, and N. C. MacDonald. Upper and lower bounds for programmable vector fields with applications to MEMS and vibratory plate parts feeders. In *International Workshop on Algorithmic Foundations of Robotics (WAFR)*, Toulouse, France, July 1996. `http://www.cs.cornell.edu/home/karl/MicroManipulation`.

[8] K.-F. Böhringer, B. R. Donald, R. Mihailovich, and N. C. MacDonald. Sensorless manipulation using massively parallel microfabricated actuator arrays. In *Proc. IEEE Int. Conf. on Robotics and Automation (ICRA)*, pages 826–833, San Diego, CA, May 1994. `http://www.cs.cornell.edu/home/karl/MicroManipulation`.

[9] G. Boothroyd, C. Poli, and L. E. Murch. *Automatic Assembly.* Marcel Dekker, Inc., 1982.

[10] R. Brooks. A layered intelligent control system for a mobile robot. *IEEE Journal of Robotics and Automation*, RA(2), 1986.

[11] M. E. Caine. *The Design of Shape from Motion Constraints.* PhD thesis, Massachusetts Institute of Technology, Department of Computer Science, 1993.

[12] J. Canny and K. Goldberg. "RISC" for industrial robotics: Recent results and open problems. In *Proc. IEEE Int. Conf. on Robotics and Automation (ICRA)*. IEEE, May 1994.

[13] Y. Chitour, A. Marigo, D. Prattichizzo, and A. Bicchi. Polling polyhedra on a plane, analysis of the reachable set. In *International Workshop on Algorithmic Foundations of Robotics (WAFR)*, Toulouse, France, July 1996.

[14] E. F. Chladni. *Entdeckungen über die Theorie des Klanges.* Weidmanns Erben und Reich, Leipzig, 1787.

[15] B. R. Donald. The complexity of planar compliant motion planning with uncertainty. *Algorithmica*, 5(3):353–382, 1990.

[16] B. R. Donald, J. Jennings, and D. Rus. Information invariants for distributed manipulation. In K. Goldberg, D. Halperin, J.-C. Latombe, and R. Wilson, editors, *International Workshop on Algorithmic Foundations of Robotics (WAFR)*, pages 431–459, Wellesley, MA, 1995. K. Peters.

[17] B. R. Donald and P. Xavier. Provably good approximation algorithms for optimal kinodynamic planning for cartesian robots and open chain manipulators. *Algorithmica*, 14(6):480–530, Nov. 1995.

[18] M. A. Erdmann. An exploration of nonprehensile two-palm manipulation: Planning and execution. Technical report, Carnegie Mellon University, Pittsburgh, PA, 1996.

[19] M. A. Erdmann and M. T. Mason. An exploration of sensorless manipulation. *IEEE Journal of Robotics and Automation*, 4(4), Aug. 1988.

[20] M. A. Erdmann and M. T. Mason. Nonprehensile manipulation. In *International Workshop on Algorithmic Foundations of Robotics (WAFR)*, Toulouse, France, July 1996.

[21] G. T. Farnum and B. Davis. Delivering the part. *Manufacturing Engineering*, March 1986.

[22] K. Y. Goldberg. Orienting polygonal parts without sensing. *Algorithmica*, 10(2/3/4):201–225, August/September/October 1993.

[23] D. D. Grossman and M. W. Blasgen. Orienting mechanical parts by computer-controlled manipulator. *IEEE Trans. on Systems, Man, and Cybernetics*, 5, 1975.

[24] J. Hartley. Picking parts from a bowlfeeder with image sensing. *Sensor Review*, 1(1), January 1981.

[25] J. W. Hill. Programmable bowl feeder design based on computer vision. *Assembly Automation*, 1(1), November 1980.

[26] H. Hitakawa. Advanced parts orientation system has wide application. *Assembly Automation*, 8(3), 1988.

[27] L. E. Kavraki. On the number of equilibrium placements of mass distributions in elliptic potential fields. Technical Report STAN-CS-TR-95-1559, Department of Computer Science, Stanford University, Stanford, CA 94305, 1995.

[28] T. Lozano-Pérez, M. Mason, and R. Taylor. Automatic synthesis of fine-motion strategies for robots. *Int. Journal of Robotics Research*, 3(1), 1984.

[29] T. McGeer. Passive dynamic walking. *Int. Journal of Robotics Research*, 1990.

[30] B. Mirtich and J. Canny. Impulse-based simulation of rigid bodies. In *Symposium on Interactive 3D Graphics*, Monterrey, CA, 1995.

[31] P. Moncevicz, M. Jakiela, and K. Ulrich. Orientation and insertion of randomly presented parts using vibratory agitation. In *ASME 3rd Conference on Flexible Assembly Systems*, September 1991.

[32] J. L. Nevins and D. E. Whitney. Computer-controlled assembly. *Scientific American*, 1978.

[33] D. Pherson. Programmable feeder for non-rotational parts. In *15th CIRP International Seminar on Manufacturing Systems*, 1983.

[34] M. H. Raibert, J. K. Hodgins, R. R. Playter, and R. P. Ringrose. Animation of legged maneuvers: jumps, somersaults, and gait transitions. *Journal of the Robotics Society of Japan*, 11(3):333–341, 1993.

[35] A. Rao and K. Goldberg. Shape from diameter: Recognizing polygonal parts with a parallel-jaw gripper. *International Journal of Robotics Research*, 13(1), February 1994.

[36] J. W. S. Rayleigh. *The Theory of Sound*. Dover, New York, 2nd edition, 1945.

[37] A. H. Redford and E. Lo. *Robots in Assembly*. Halsted Press, New York, 1986.

[38] D. Reznik, S. Brown, and J. F. Canny. Dynamic simulation as a design tool for a microactuator array. In *Proc. IEEE Int. Conf. on Robotics and Automation (ICRA)*, Albuquerque, NM, Apr. 1997. Submitted for review. `http://www.cs.berkeley.edu/~dreznik/mems.html`.

[39] F. J. Riley. *Assembly Automation, A Management Handbook.* Industrial Press, New York, 1983.

[40] B.-Z. Sandler. *Robotics: Designing the Mechanisms for Automated Machinery.* Prentice Hall, 1991.

[41] B. J. Schroer. Electronic parts presentation using vibratory bowl feeders. *Robotics*, 3, 1987.

[42] N. C. Singer and W. P. Seering. Utilizing dynamic stability to orient parts. *Journal of Applied Mechanics*, 54:961–966, Dec. 1987.

[43] J. W. Suh, S. F. Glander, R. B. Darling, C. W. Storment, and G. T. A. Kovacs. Combined organic thermal and electrostatic omnidirectional ciliary microactuator array for object positioning and inspection. In *Proc. Solid State Sensor and Actuator Workshop*, Hilton Head, NC, June 1996.

[44] T. Suzuki. An approach to a flexible part-feeding system. In *1st International Conference on Assembly Automation*, 1980.

[45] P. Swanson, R. Burridge, and D. Koditschek. Global asymptotic stability of a passive juggler: A parts feeding strategy. In *Proc. IEEE Int. Conf. on Robotics and Automation (ICRA)*, Nagoya, Japan, May 1995.

[46] S. Timoshenko. *Theory of Plates and Shells.* McGraw-Hill, New York, 1940.

[47] N. D. Tran and K. W. Chan. Object behavior using a vibrating plate testbed for part presentation research. Term Paper 304-494, Electrical Engineering Department, McGill University, Dec. 1995. Instructor Vince Hayward.

[48] S. S. M. Wang and P. Will. Sensors for computer controlled mechanical assembly. *Industrial Robot*, March 1978.

[49] N. B. Zumel and M. A. Erdmann. Nonprehensile two palm manipulation with non-equilibrium transitions between stable states. In *Proc. IEEE Int. Conf. on Robotics and Automation (ICRA)*, Minneapolis, MN, Apr. 1996.